NASA Grant NGR 21-022-350

Principal Investigator - Jackson C. S. Yang
Professor

Co-principal Investigator - C. Y. Tsui
Assistant Professor

Final Report

# Optimum Design of Structures of Composite Materials in Response to Aerodynamic Noise and Noise Transimission


Submitted to

Ames Research Center
Aeronautical Structure Branch
Moffett Field, California

December 9, 1977

## Table of Contents

# INTRODUCTION

An inherent area of interest in high-speed flight such as experienced in the re-entry of the space shuttle is the creation of unusual aerodynamic fields around the space vehicle and its associated problems. High pressure fluctuations in the aerodynamic field due to attached and detached boundary layers and shock waves give rise to high structural vibrations as well as intensive acoustical atmospheres in the interior of the vehicle. The problem is two-folded. First, the creation of the boundary layers and shock waves is considered as an input to the structure of the space vehicle. Second, with the input, the response of the structure can be obtained. The determination of the structural response however, is complicated due to the random pressure loading from the turbulant boundary layer and by the acoustical transmission phenomenon. In other words, as the structure vibrates, energy is transmitted to the interior of the space vehicle, and the rate of energy transmission and sound intensity are governed by the mechano-acoustical boundary condition of the interior structural boundary. One simplication is often taken here. This is to ignore the coupling effects and solve for the structural vibration based on the input. The interior acoustical condition is solved separately by considering sound transmission through the structure from an acoustical input equivalent to the input pressure fluctuation within the boundary layer.

The determination of the pressure fluctuation within the boundary layer has been investigated previously by many researchers.

Publications are numerous including theoretical treatments by Lighthill (1), Phillips (2), and Ribner (3) and experimental investigations by Chyu and Hanly (4), Coe (5) and Bull and Willis (6). Through these efforts, it can now reasonably assert that the input pressure fluctuation is known.

The solution of the structural vibration is not so assured. This is due to the requirement for light weight material with great strength and stiffness for the structure. New materials are contemplated whose behavior under dynamic loading has not been fully understood to warrant their application in actual flight. One promising material is the composite materials such as epoxy reinforced by carbon fibers. It is interesting to study the effect of those parameters such as modulus of elasticity (ratio of fiber to matrix), fiber size and orientation, matrix strength, dissipative characteristics, etc., so that optimum structural design for vibratory input can be obtained. The same material is also examined for noise transmission characteristics.

The tasks for the present grant can be summarized as follows:

1. The investigation of elastic wave propagation and attenuation in a model fiber - matrix .
2. The measurement of damping characteristics in graphite epoxy composite material.
3. The construction of a sound transmission test facility suitable to incorporate into NASA Ames wind tunnel for measurement of transmission loss due to sound generation in boundary layers.
4. The measurement of transmission loss of graphite epoxy composite panels.

## RESULTS

The results of the investigation of the task assignments mentioned in the last section are briefly mentioned here. More formal and complete results in the form of journal publications and other presentations are given in the Appendix.

1. Elastic Wave Propagation in a Model Fiber-Matrix

The model chosen for this experiment was a metal plate fitted with cylindrical inclusions of a different metal to resemble fiber elements in a homogeneous matrix material. The input was simulated by a sharp pulse executed by explosive or the impingement of a sharp knife-edged ram. The application of the pulse was at the edge of the plate such that the ensuing elastic waves propagated in a direction perpindicular to its inclusions. The propagation of the waves were monitored by strain gages.

Theoretical analysis was performed using Fermat's principle of the ray theory where the location of the wave fronts with respect to time was obtained. The composite solution was compared to experimental results and was found to correlate well. This presented concrete evidence that the analytical method can be used in fiber reinforced composite material analysis.

This part of the project has supported one graduate student to complete his MSME thesis entitled "Theoretical and Experimental Investigation of Stress Wave Attenuation in Model of Fiber Reinforced Composite Material" (by Y. Ueng, 1972) and resulted in an AIAA Journal publication (Volume II, No. 4, pp. 472-477, April 1973) by its Principal and Co-principal investigators. A copy of the

reprint of the journal article is included in the Appendix. Preliminary result of the investigation was also presented in the 13th AIAA/ASME/(SAE Structures, Structural Dynamics and Material Conference, San Antonio Texas, April 10-12, 1972).

2. Measurement of Damping Characteristics in Graphite Epoxy Materials

A technique called random decrement was developed which makes possible the computation of damping values as well as the detection of damage in structure when only response data is available. Using this technique, damping ratios were computed for several modes of randomly excited graphite-epoxy panels. The random input was induced by speakers within one of the twin reverberation chamber built for this project. Response data were obtained from miniature accelerometers attached to the panel.

This part of the project has supported one graduate student to complete his MSME thesis entitled "The Measurement of Damping and the Detection of Damage in Structures by the Random Decrement Technique" (by D. Caldwell, 1975) and resulted in a paper entitled "Measurement of Damping in Composite Beams and Plates." Published in the 46th Shock and Vibration Bulletin, Nov. 1975, with D. Caldwell. See Appendix. The result of research indicated that the damping ratios compared well to those which were derived from power spectral density method. Further work on the response of plates due to random pressure loading from a turbulent boundary layer was also coordinated which resulted in a presentation in the Navy-NASTRAN Colloqueum, Bethesda, Maryland, September 1974 and published in the Proceedings of the Fifth Navy-NASTRAN Colloqueum, pp.81-86. See Appendix.

3. Sound Transmission Test Facility

The sound transmission test facility was designed to attach to one of NASA Ames wind tunnel to allow for sound transmission loss measurements through a composite panel. One side of the panel was designed to fit flush with the interior of the wind tunnel and become a part of the walls. Sound generation within the boundary layer was transmitted through the composite panel and the transmission loss was obtained in sites by this manner.

The facility constructed was a set of twin reverberation chambers made with plywood frame and masonite interior. The chambers were shaped like a five-sided parallelepiped with an inclined roof to facilitate sound reflections in the interior. Opening was made at one of the side walls to fit a composite panel 16" by 16" in size. The sound transmission area was 12" x 12". The chamber, having an internal volume of 48 cubic feet with corresponding surface area of 83 square feet was adequate for sound transmission loss measurement at input frequencies above 400 Hz.

This part of the project has supported one graduate student to complete his MSME thesis titled "Design, Construction, and Performance of a Small Reverberation Chamber for Transmission Loss Measurements" (by C. Voorhees, 1974) and resulted in a journal publication co-authored by the Principal, Co-principal Investigators and the graduate student (Applied Acoustics #9, 1976, pp. 165-175). A copy of the reprint of the journal article is included in the Appendix. Preliminary result of the investigation was presented in the 87$^{th}$ Meeting of the Acoustical Society of America, New York, NY, April 23-26, 1974. The abstract of the presentation

appears in the Journal of Acoustical Society of America Vol 55, Supplement, p. 513, 1974.

The test facility was not put to use in the NASA Ames wind tunnels due to scheduling difficulties.

4. Measurement of Transmission Loss of Composite Panels

The sound insulation property of several composite material panels were measured. The panels were placed between the twin reverberation chambers. Bands of third octane sound were generated by speakers placed in the source room. The transmission loss for each panel was obtained by modifying the noise reduction across the panel, taking into account the absorptive power of the walls of the receiving room. The results for three composite panels are presented in Figure 1. These were graphite epoxy composite panels 0.038" thick. Each panel was made of eight laminations with the graphite fibers orientated respectively at ±45°, ±22.5° and 0-90° to one of the edges. Experimental results showed that the panels behaved very similarly to one with homogeneous structure such as common aluminum panels. In the upper audible range from 500 Hz to ultrasonic, the behavior of the panels is governed by the limp-wall law. A comparison of the transmission loss of a 0.039" graphite epoxy composite panel to one of 0.026" aluminum panel, both of same surface density are given in Figure 2. Thus the composite panel, due to its high rigidity, may have an advantage in reduction of structural vibration, but its light weight have not resulted in an improvement of sound insulation characteristic. This finding should prove useful to NASA space vehicle designers responsible in reduction of cabin noise during space flight.

Fig. 1 Transmission Loss of Graphite - Epoxy Panels at Various File Orientations

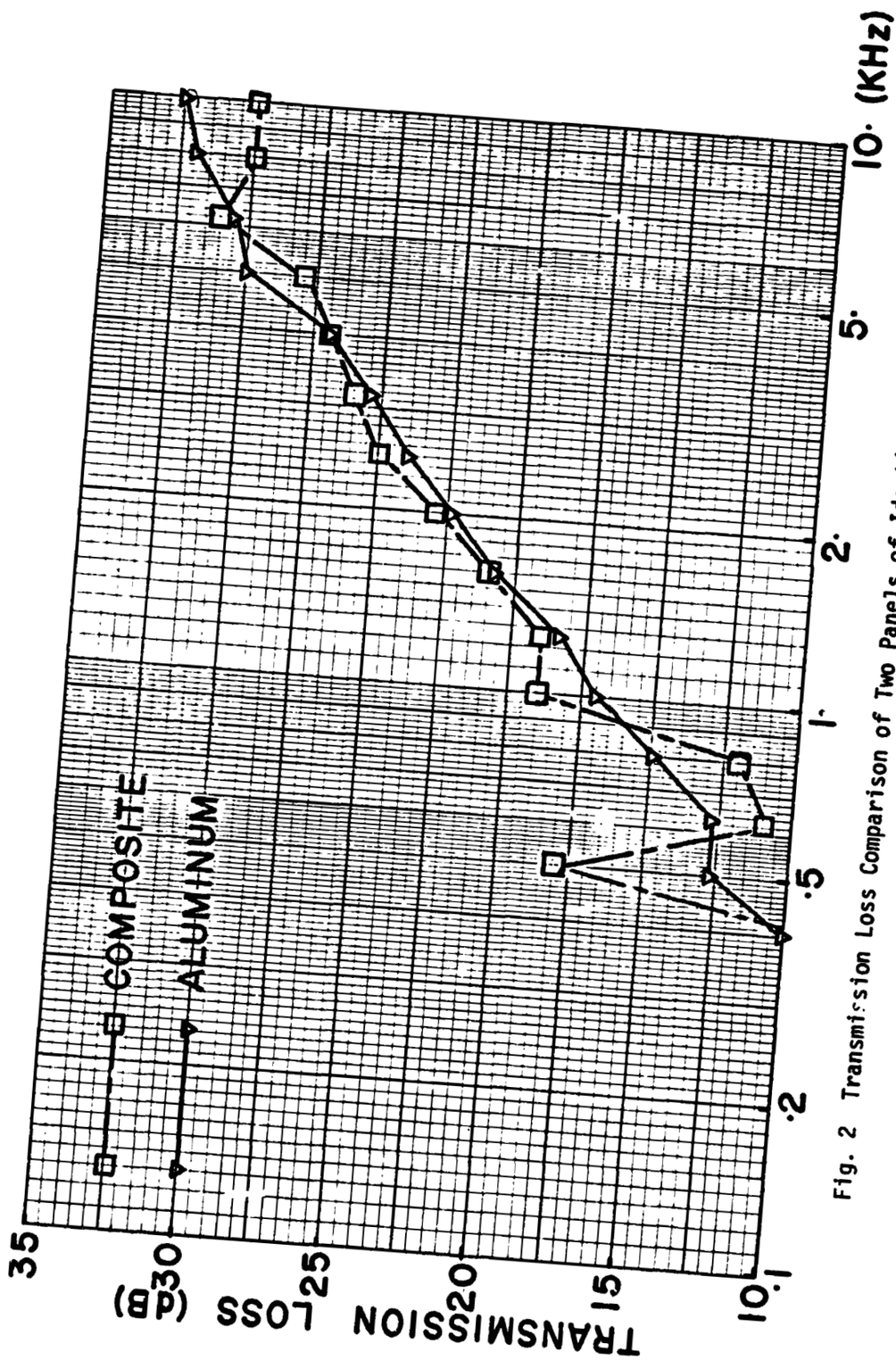


Fig. 2 Transmission Loss Comparison of Two Panels of Identical Surface Density

## REFERENCES

1. Lighthill, M.J. "On Sound Generated Aerodynamically. I. General Theory", Proc. Roy. Soc. Ser. A, Vol 211, 1952 pp. 564-578.

2. Phillips, O.M. "On the Generation of Sound by Supersonic Turbulent Shear Layers", Journal of Fluid Mechanics, Vol. 9, 1960, pp. 1-28.

3. Ribner, H.S. "The Generation of Sound by Turbulent Jet", Vol. 8 of Advances in Applied Mechanics, Academic Press, Inc. 1964, pp. 103-182.

4. Chyu, W.J. and Hanly, R.D. "Power and Cross-Spectra and Space-Time Correlations of Surface Fluctuating Pressures at Mach Numbers Between 1.6 and 2.5", AIAA paper no. 68-77, Jan. 1968.

5. Coe, C.F. "Surface-Pressure Fluctuations Associated with Aerodynamic Noise", NASA AP-207, July, 1969 pp. 409-424.

6. Bull, M.K. and Willis, J.L. "Some Results of Experimental Investigations of the Surface Pressure Field Due to a Turbulent Boundary Layer", AASU Rept. 199, Nov. 1961.

# APPENDICES

A. Experimental and Theoretical Investigation of Stress Wave Attenuation by Inclusions

B. Measurement of Damping in Composite Beams and Plates

C. Response of Plates to Random Pressure Loading from a Turbulent Boundary Layer

D. The Design of Small Reverberation Chambers for Transmission Loss Measurement

# Appendix A

# Experimental and Theoretical Investigation of Stress Wave Attenuation by Inclusions

J. C. S. YANG AND C. Y. TSUI
*University of Maryland, College Park, Md.*

*Reprinted from* **AIAA Journal**

Volume 11, Number 4, Pages 472-477, April 1973

*Reprinted from* AIAA JOURNAL, Vol. 11, No. 4, April 1973, pp. 472-477


# Experimental and Theoretical Investigation of Stress Wave Attenuation by Inclusions

J. C. S. YANG* AND C. Y. TSUI†
*University of Maryland, College Park, Md.*

**The propagation of an initially sharp cylindrical pressure pulse through a linear elastic medium with inclusions is analyzed, both experimentally and analytically. In the experiment, tests were performed on plates with single and multiple circular inclusions embedded in a matrix of lower characteristic impedance. Sharp compression pulses were generated at an edge of the plate by two methods; the detonation of a charge of lead azide and the impingement of a sharp knife-edged ram impacted at the opposite end by a short projectile. Strain gages were mounted on various positions of the plate to determine the attenuation of the transient stress. The qualitative analytical treatment is based on the methods of propagating stress discontinuities. Computer programs were written to numerically determine the changes in the shape of the leading wave front and the stresses immediately behind it. Experimental results for the attenuation of stress wave on steel-aluminum and steel-brass inclusion-matrix composites compared very well with the computed analytical results.**

## Introduction

GROWING requirements for lightweight materials with great strength and stiffness, especially in the aerospace field on such projects as STOL, VTOL aircraft, Space Shuttle vehicles, heat shield, etc., have led to increased interest and research in the area of fiber composite materials.

One of the most interesting properties of fiber-reinforced composites is their dispersive characteristics. In general, when a stress pulse is applied to the boundary of a composite, the shape of the pulse is changed, and it "smears out" as it propagates through the slab, with an attenuation of amplitude. Thus the composite appears to have greater dynamic than static strength. However, for dynamic loads, the simplest geometrical configuration may give rise to tensile stresses, even though the loading is compressive. The load-carrying capacity of a body fabricated on a fiber-reinforced composite is adversely affected by bond failure at the interface bonds; in particular, it may be substantially smaller than the strengths of the materials constituting the composite, and relatively small tensile stresses may thus produce bond failure. In addition, fracture and spallation could occur due to the reflection at the back free surface of the slab, and internal stress concentration could occur due to refractions, reflections, and a focusing effect of the geometrical configuration. Few analytical and experimental investigations of such situations appear to have been carried out. In many cases, it is believed that the development of composites has proceeded with little appreciation for the importance of microstructural variables such as interface strength, modulus ratios, fiber size, etc., on the composite strength under stress-wave loading. Consequently, in order to have increased resistance to stress-wave fracture, a better understanding of the micromechanics of the fracture process must be developed. This approach is necessary to guide composite material development, and should result in large-scale practical benefits.

In this paper, we are concerned with the propagation of an initially sharp cylindrical pressure pulse through a linear elastic medium with inclusions. The pattern of transient waves is extremely complicated, and for the analytical treatment, the attention is, therefore, focused on the changes in the shape of the leading wave front and the stress immediately behind it.

The basis for the present approach is the ray tracing and associated wave front analysis of geometrical optics. It can be shown that even in the case of elastic waves with two basic wave speeds in each material, the stress amplitude at the initial

Presented as Paper 72-394 at the AIAA/ASME/SAE 13th Structures, Structural Dynamics, and Materials Conference, San Antonio, Texas, April 10-12, 1972; submitted April 25, 1972; revision received September 22, 1972. This work was jointly supported by NASA Ames Research Center under contract NGR-21-002-350; the Minta Martin Fund, College of Engineering and the Computer Science Center, University of Maryland.

Index categories: Structural Dynamic Analysis; Structural Composite Materials (Including Coatings).

* Professor. Member AIAA.

† Assistant Professor.

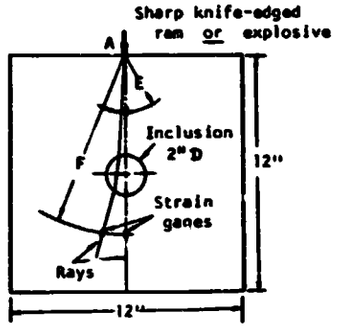


Fig. 1 Single inclusion specimen.

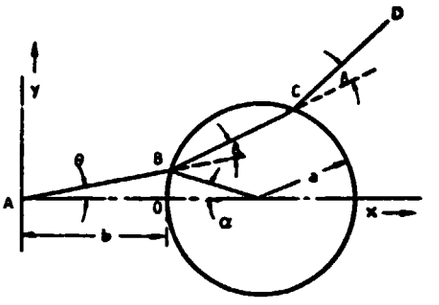


Fig. 3 Geometrical parameters for computation of the wave front.

wave front is given exactly by the law of geometrical optics associated with the propagation of irrotational waves. This follows from application of the theory of characteristics and is in accordance with the more common interpretation of geometrical optics as an approximation to the solution for oscillatory waves at high frequencies. This approach determines the stress tensor at the wave front, and can be extended also to determine stress gradients there.

The propagation of stress discontinuities was discussed in considerable detail by Thomas.[1] Much of the recent work in this area is patterned after that due to Luneburg,[2] for electromagnetic discontinuities, and Friedlander,[3] for the propagation of discontinuities in acoustic media. Propagation of stress discontinuities in elastic media, including the reflections and refractions of discontinuities at interfaces of different elastic solids, was investigated by Keller.[4] An application of wave-front analysis to the problem of an inclusion embedded in an elastic medium was presented by Ting and Lee.[5] Achenbach, Hemann, and Ziegler[6] presented an interesting experiment in studying separation of the interface of a circular inclusion and the surrounding medium. Nariboli[7] combined the ideas of the theory of singular surfaces with those of ray theory. Recently, Ben-Amoz[8] considered the problem of propagation of actual stress pulses through bounded anisotropic media.

## Experiments

The specimen used for the experiment consisted of 12 in.$^2$ plates made of aluminum or brass with steel inclusions. The inclusions were shrunk fit in the plate with an interface pressure of approximately 200 psi. The steel-aluminum combination has a characteristic impedance ratio of 2.66 and a propagation velocity ratio of 1.03, and the steel and brass have ratios of 1.27 and 1.39, respectively. Four different kinds of specimens were tested—i.e., one, two, three, and four cylindrical inclusions with the total area kept equal. A drawing of a single-inclusion specimen is shown in Fig. 1. In addition, experiments were also conducted on 12 in. × 12 in., 12 in. × 48 in., and 48 in. × 48 in. aluminum plates without inclusion.

The compressive pulse in the plate was generated by two methods: 1) The detonation of lead azide at the center of the upper edge (The plates were placed in a vertical position and supported by rubber pads at the lower corners.); and 2) The impingement of a knife-edged ram (The specimens were supported freely on rollers with the center of one edge resting against the ram. The other end of the ram was impacted by a projectile released from an air gun.) A schematic diagram of this experimental arrangement is given in Fig. 2.

Both the lead azide charge and the impingement of the sharp ram produced cylindrical waves emanating from the edge at the point of contact into the plate. During the experiment, different amounts of lead azide and several impact velocities and projectile lengths were used. Pairs of strain gages were mounted on the opposite faces of the plate at various positions along the rays (see Fig. 1) to measure the transient stress. Each pair of gages are connected in the opposite arms of a wheatstone bridge circuit to cancel any bending effects. The output signal from the bridge circuit was fed into an oscilloscope.

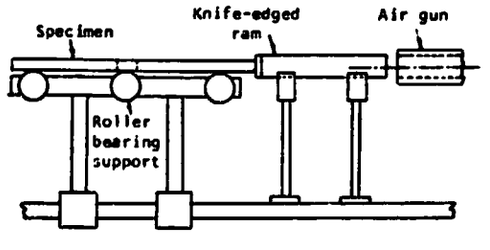


Fig. 2 Experimental arrangement for generation of pulse by impingement of a knife-edged ram.

## Analysis

The wave fronts can be located by a direct calculation using Fermat's principle. To illustrate the procedure in computing rays and wave front, let us consider a ray AB in Fig. 3 which strikes the inclusion at angular position $\theta$. For simplicity, distortion wave fronts are omitted and only the rays associated with a compressive wave front are sketched. If $a$ is the radius of the inclusion and $b$ the distance from the applied pressure point to the inclusion, the coordinates of point B are given by $x_B = L_{AB}\cos\theta$ and $y_B = L_{AB}\sin\theta$, where $L_{AB}$ is the length of the straight ray AB and is given by

$$L_{AB} = (b+a)\cos\theta - [(b+a)^2\cos^2\theta - b^2 - 2ab]^{1/2}$$

Let $t = 0$ be the time at which the cylindrical wave initiates at $x = 0$. The time $t$ required for the wave front to reach point B

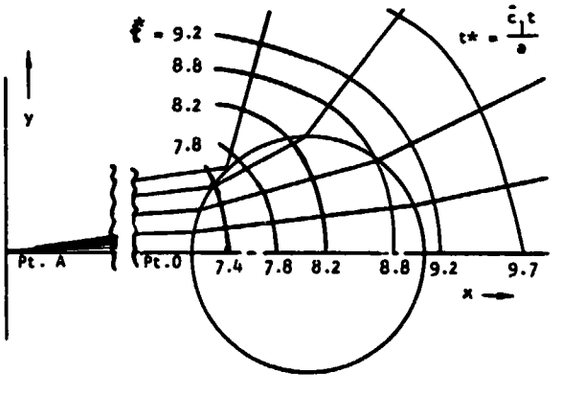


Fig. 4 Wave front for cylindrical inclusion.

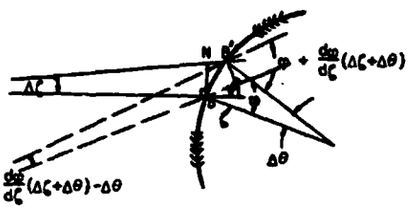


Fig. 5 Refraction of two neighboring rays.

is $t = L_{AB}/c_1$, where $c_1$ is the speed of longitudinal waves in medium 1. The time $t$ required for point C on the refracted ray BC to be reached by the wave front is

$$t = L_{AB}/c_1 + L_{BC}/c_2, \quad \text{or} \quad L_{BC} = c_2(t - L_{AB}/c_1)$$

where $L_{BC}$ is the length of the straight ray BC and $c_2$ is the speed of longitudinal waves in medium 2. The inclination of the refracted ray to the incident ray direction, $\delta$, is given by Snell's Law

$$c_1/c_2 = \sin\zeta/\sin\phi \tag{1}$$

where $\zeta = \theta + \alpha$ and $\phi = a + \theta + \delta$.

The coordinates of point C are given by $x_C = x_B + L_{BC}\cos(\theta+\delta)$ and $y_C = y_B + L_{BC}\sin(\theta+\delta)$, where the length $L_{BC}$ can also be expressed by $L_{BC} = 2a\cos\phi$.

A similar calculation determines the wave front after refraction out of the inclusion. The coordinates of point D are given by

$$x_D = x_C + L_{CD}\sin(\theta+2\delta) \quad \text{and} \quad y_D = y_C + L_{CD}\sin(\theta+2\delta)$$

where $L_{CD}$, the length of the straight ray $CD$, is determined by

$$t = L_{AB}/c_1 + L_{BC}/c_2 + L_{CD}/c_1 \quad \text{or} \quad L_{CD} = c_1 t - L_{AB} - c_1/c_2 L_{BC}.$$

The wave fronts as expressed by the aforementioned equations are shown in Fig. 4 for various times.

A complete analytical treatment of the stresses for the wave propagation problem shown in Fig. 1 is very difficult. However, the stresses at the instant that the wave fronts arrive can be obtained in a rather straightforward and simple manner by investigating propagating stress discontinuities. The analysis assumes linear elastic response of the materials of the inclusion and the matrix. In addition, it is assumed that the applied pressure instantaneously rises to a certain value and then rapidly decreases to zero. The stress discontinuity applied on the boundary generates surfaces of discontinuity which propagates into the interior of the continuous body in a manner which was discussed by other authors, most notably by Thomas[1] and Keller.[4] Here we consider the problem in two spatial dimensions. When given the initial signal at a point on each ray, the variation of this signal along the ray is governed by

$$p^2 R = \text{const} \tag{2}$$

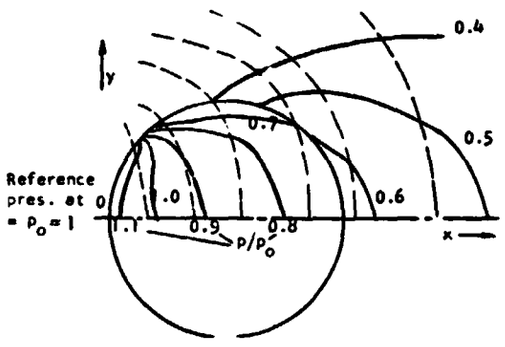


Fig. 6 Pressure at wave front for cylindrical inclusion.

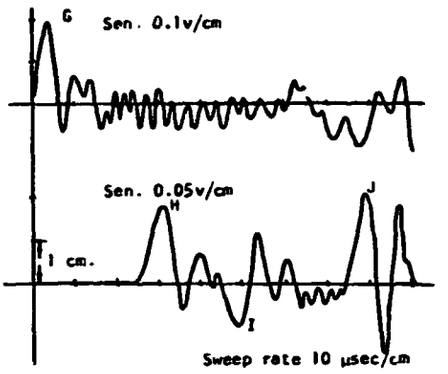


Fig. 7 Reproduction of strain histories due to explosive loading on a single-inclusion steel-aluminum specimen, 0° ray.

Changes in intensity at the boundary between the matrix and inclusions are determined by the equivalent of Fresnel's formulas for elastic media.[9] The pressure ratio at the interface can be written in the following form:

$$\frac{\bar{p}}{p} = \frac{\bar{\rho}(\bar{c}_1^{\,2} - 4\bar{c}_2^{\,2}/3)c_1^{\,2}}{\rho(c_1^{\,2} - 4c_2^{\,2}/3)\bar{c}_1^{\,2}} \cdot \frac{3M\cos\zeta}{KM + LN} \tag{3}$$

where

$$K = \cos\zeta\left(\frac{\bar{\rho}}{\rho} + n\sin\zeta\right)\frac{c_1}{\bar{c}_1}\left[1 - \left(\frac{\bar{c}_1}{c_1}\sin\zeta\right)^2(1 - n\sin^2\zeta)\right]^{1/2}$$

$$M = \left(\frac{\bar{\rho}}{\rho} + n\sin^2\zeta\right)\frac{c_2}{\bar{c}_2}\left[\frac{1 - (\bar{c}_2/c_1)^2\sin^2\zeta}{1 - (c_2/c_1)^2\sin^2\zeta}(1 - n\sin^2\zeta)\right]^{1/2}$$

$$L = \frac{c_2}{c_1}\frac{\sin\zeta}{\left[1 - \left(\frac{c_2}{c_1}\sin\zeta\right)^2\right]^{1/2}}\left(1 = \frac{\bar{\rho}}{\rho} - n\sin^2\zeta\right) -$$

$$\frac{c_1}{\bar{c}_1} \quad \cdot 1\,\zeta\left[1 - \left(\frac{\bar{c}_1}{c_1}\sin\zeta\right)^2\right]^{1/2}$$

$$N = \left(1 - \frac{\bar{\rho}}{\rho} - n\sin^2\right)\sin\zeta - \frac{c_1}{\bar{c}_2}n\sin\zeta\cos\zeta \times$$

$$\left[1 - \left(\frac{\bar{c}_2}{c_1}\sin\zeta\right)^2\right]^{1/2}$$

$$n = 2\left[\left(\frac{c_2}{c_1}\right)^2 - \frac{\bar{\rho}}{\rho}\left(\frac{\bar{c}_2}{c_1}\right)^2\right]$$

The quantities with a bar refer to the inclusion whereas the quantities without a bar refer to the matrix.

Let $\bar{p}_B$ and $p_B$ be pressure at point B in Fig. 5 on the side of medium 2 and medium 1 respectively.

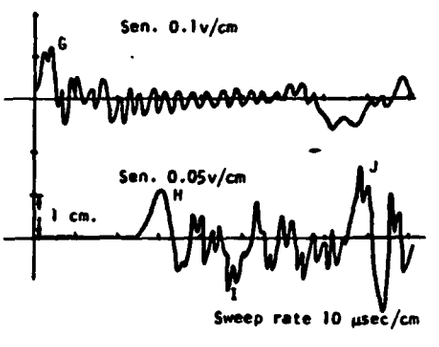


Fig. 8 Strain histories of an equivalent plate as the steel-aluminum specimen except without the steel inclusion.

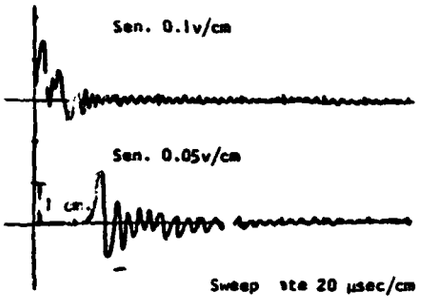


Fig. 9 Disappearance of peaks due to reflected waves in the strain histories of a large aluminum plate.

The pressure $p_B$ can be determined by using Eq. (2)

$$p_B = p_0[b/L_{AB}]^{1/2}$$

where $p_0$ is the pressure at point 0 and $b$ is the length of the straight ray AO, and the refracted pressure $\bar{p}_B$ can then be determined by using Eq. (3). Then, Eq. (2) is used to relate points B and C

$$\bar{p}_C/\bar{p}_B = [\bar{R}_B/\bar{R}_C]^{1/2}$$

where $\bar{R}_B$ is the radius of curvature of the wave fronts at point B in medium 2, and $\bar{R}_C$ is the radius of curvature of the wave front at point C in medium 2. The radius of curvature, $\bar{R}_B$, of the refracted wave fronts at point B can be obtained by considering two neighboring points on the interface, B and B′ as shown in Fig. 5. The angle of refraction at B′ is

$$\phi_{B'} \sim \phi + (d\phi/d\zeta)(\Delta\zeta + \Delta\theta)$$

From Snell's law [Eq. (1)], we find $d\phi/d\zeta = \tan\phi/\tan\zeta$.

The following relations are deduced from Fig. 5:

$$\Delta\zeta = \mathrm{BN}/L_{AB}, \quad \Delta\theta = \overline{\mathrm{BB}'}/a,$$

and

$$(d\phi/d\zeta)(\Delta\zeta + \Delta\theta) - \Delta\theta = \overline{\mathrm{B'M}}/\bar{R}_B$$

Also $\mathrm{BN} = \overline{\mathrm{BB}'}\cos\zeta$, $\overline{\mathrm{B'M}} = \overline{\mathrm{BB}'}\cos\phi$. After substituting and simplifying, we obtain:

$$\bar{R}_B = \cos\phi\left[\frac{\tan\phi}{\tan\zeta}\left(\frac{\cos\zeta}{L_{AB}} + \frac{1}{a}\right) - \frac{1}{a}\right]^{-1}$$

Since the rays are straight lines normal to the wave front in both medium we obtain

$$\bar{R}_C = \bar{R}_B + L_{BC}$$

The pressure $p_C$ can be determined from Eq. (3) where $p_C$ is the pressure at point C after being refracted out of the inclusion to the matrix. Then using Eq (2)

$$p_D/p_C = [R_C/R_D]$$

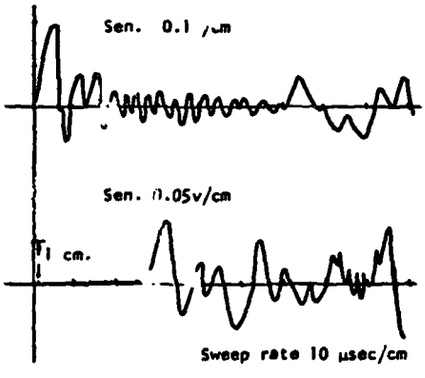


Fig. 10 Strain histories due to explosive loading on a single-inclusion steel-aluminum specimen, 5° ray.

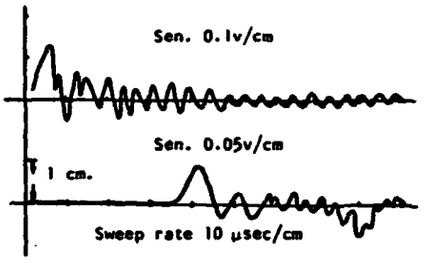


Fig. 11 Strain histories due to explosive loading on a single-inclusion steel-brass specimen, 0° ray.

The derivation of the radius of curvature $R_C$ follows the same procedure as before:

$$R_C = \cos(\phi+\delta)\left[\frac{\tan(\phi+\delta)}{\tan\phi}\left(\frac{\cos\phi}{\bar{R}_C} - \frac{1}{a}\right) + \frac{1}{a}\right]^{-1}$$

Again, since the rays are straight lines normal to the wave front in each medium, $R_D = R_C + L_{CD}$.

Figure 6 shows an example of the pressure $p$ as a function of position when the wave front arrives. The results are shown in the form of contour lines of constant pressure. The material constants used are $c_2/c_1 = 1.39$, and characteristic impedance ratio = 1.27. The pressure at point 0 is taken to be unity. Figure 6, when used in conjunction with Fig. 4, enables one to determine the pressure at the wave front for a given $t$. The wave fronts obtained in Fig. 4 are also shown in Fig. 6. Clearly, one can continue this procedure to determine the wave fronts and the pressure at the wave fronts for more than one inclusion.

## Results

The magnitude and shape of the experimental strain histories were plotted from typical oscilloscope traces. A sample plot for the aluminum specimen with a single steel inclusion is shown in Fig. 7. The result was due to the detonation of a charge of lead azide at point A (see Fig. 1). The upper and lower traces correspond to the strain measured by the two pairs of strain gages which are located along the 0° ray, 4 in. and 10 in. from the point of detonation. The center of the 2-in.-diam inclusion is midway between the gages.

A rise time of 4 μsec was observed on both traces for the pressure pulse to reach its peaks $G$ and $H$. The delay time of 29 μsec for the arrival of the pressure pulse between the gages correlated very well with the theoretically computed delay time of 29.5 μsec. The amplitude ratio of the peak strain, $H/G$, for the two strain gage measurements is 0.52. This compared very well with the amplitude ratio of 0.55 calculated from the ray theory. Another experiment was conducted on a specimen of the same dimension except without the inclusion. The result is shown in Fig. 8. The amplitude ratio of the peak strains, $H/G$, is 0.60

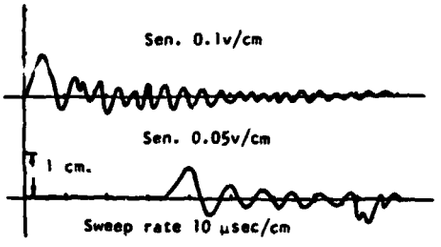


Fig. 12 Strain histories due to explosive loading on a single-inclusion steel-brass specimen, 4° ray.

Table 1 Summary of results

| | Material | Location of strain gages, in. | Inclusions | Ray $\theta$, deg | Peak amplitude ratio, $H/G$ | |
|---|---|---|---|---|---|---|
| | | | | | Experimental | Theoretical |
| I Explosive | Steel-aluminum | E = 4 | 1 | 0 | 0.52 | 0.55 |
| | | F = 10 | | 5 | 0.46 | 0.52 |
| | | E = 3 | 1 | 0 | 0.45 | 0.43 |
| | | F = 9 | | 4 | 0.47 | 0.42 |
| | Steel-Brass | E = 1.8 | 2 | 0 | 0.29 | 0.315 |
| | | F = 9 | | | | |
| | | E = 2.4 | 3 | 0 | 0.31 | 0.34 |
| | | F = 10 | | | | |
| | | E = 2.4 | 4 | 0 | 0.50 | 0.56 |
| | | F = 10 | | | | |
| II Ram impingement | Steel-aluminum | E = 3 | 1 | 0 | 0.53 | 0.55 |
| | | F = 10 | | | | |
| | | E = 3 | 1 | 0 | 0.42 | 0.43 |
| | | F = 9 | | | | |
| | Steel-Brass | E = 1.8 | 2 | 0 | 0.32 | 0.315 |
| | | F = 9 | | | | |
| | | E = 2.4 | 3 | 0 | 0.34 | 0.34 |
| | | F = 10 | | | | |
| | | E = 2.4 | 4 | 0 | 0.50 | 0.56 |
| | | F = 10 | | | | |
| III | Aluminum | E = 4 | 0 | | 0.60 | 0.63 |
| | | F = 10 | | | | |
| | | E = 3 | 0 | | ... | 0.57 |
| | | F = 9 | | | | |
| | | E = 2.4 | 0 | | ... | 0.49 |
| | | F = 10 | | | | |
| | | E = 1.8 | 0 | | ... | 0.445 |
| | | F = 9.0 | | | | |



as compared with a theoretically calculated value of 0.63. The delay time between the two gages again correlated well with the theoretically computed delay time. It should be noted that the amplitude ratio of the peak strains has been attenuated from 0.60 to 0.50 for the plate with the inclusion.

The strain variation at the location of each gage is also analyzed as a function of time. However, the calculation gets very complicated with the existence of the reflected and refracted waves. When there exists a large number of interfaces as in the cases of specimens with multiple inclusions or specimens with small overall dimensions, the calculation becomes virtually impossible and some effective modulus theory must be used. The pulse reflection from the back free surface is also shown in Figs. 7 and 8 with the peak tensile amplitude $I$. The rather high peak amplitude $J$ can be attributed to the multiple reflections along the 0° ray and to the reflections from the sides of the square plate which arrived at the second gage approximately, 90 μsec after the initial detonation of the charge. Both peaks, $I$ and $J$ appeared during tests on plates of the same dimension with or without the inclusion; and disappeared during tests on a similar plate but with a dimension of 48 in. × 48 in. as can be seen from Fig. 9.

Additional sample results are presented in Figs. 10–14. Figure 10 gives the strain histories of the same steel-aluminum specimen along a 5° ray. Figures 11 and 12 are the results for a steel-brass plate with one inclusion along rays $\theta = 0°$ and 4°. Figure 13 presents the strain histories for a steel-brass plate with two inclusions.

While the above are the results due to explosive loading, the strain histories of the steel-brass plate with a single inclusion

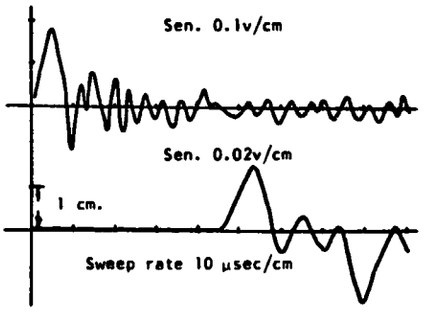


Fig. 13 Strain histories due to explosive loading on a two-inclusion steel-brass specimen, 0° ray.

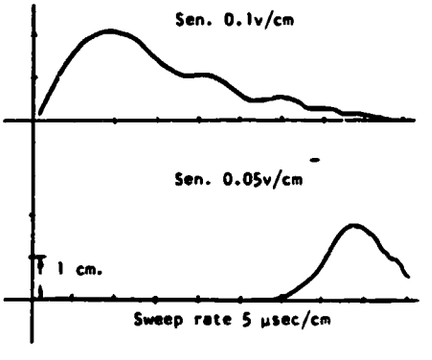


Fig. 14 Strain histories due to impingement loading on a single-inclusion steel-brass specimen, 0° ray.

due to impingement of the ram against the plate at A (see Fig. 1) are presented in Fig. 14. The risetime has a much larger value of 10 $\mu$sec compared to 4 $\mu$sec for the explosive loading.

Additional experiments using both methods were performed on plates with two, three, or four inclusions. The results of all the experiments are summarized in Table 1.

Table 1 is divided into three parts. Parts I and II refer to the two methods of pulse generation. Part III lists the theoretically computed peak ratios, $H/G$ for several selected gage locations. The results are based on Eq. (2) and are for homogeneous material. The first four columns in Table 1 give, respectively, the composites tested, the location of the strain gages, the number of inclusions, and the identity of the rays. The last two columns give the average experimental results and the results obtained by the ray theory presented in this paper.

## Conclusion

Experimental results on steel-aluminum and steel-brass inclusion-matrix composites using explosives and ram impingement compared very well with the analytically computed results using ray theory.

With good agreement between the experimental and theoretically computed results, one can confidently proceed in applying the theory to fiber-reinforced composites to determine the optimum micro-structural variables such as modulus of elasticity ratio (fiber to matrix), relative fiber size, and orientation to increase resistance to stress fracture.

## References

[1] Thomas, T. Y., *Plastic Flow and Fracture in Solids*, Academic Press, New York, 1964.

[2] Luneburg, R. K., *Mathematical Theory of Optics*, University of California Press, Los Angeles, Calif., 1964.

[3] Friedlander, F. G., *Sound Pulses*, Cambridge University Press, Cambridge, Mass., 1958.

[4] Keller, H., "Propagation of Stress Discontinuities in Inhomogeneous Elastic Media," *SIAM Review*, Vol. 6, No. 4, Oct. 1964, pp. 356–382.

[5] Ting, T. C. T. and Lee, E. H., "Wave Front Analysis in Composite Materials," *Journal of Applied Mechanics*, Vol. 36, Sept. 1969, pp. 497–504.

[6] Achenbach, J. D., Hemann, J. H., and Ziegler, F., "Separation at the Interface of a Circular Inclusion and the Surrounding Medium Under an Incident Compressive Wave," *Journal of Applied Mechanics*, Vol. 37, Ser. E, June 1970, pp. 298–304.

[7] Nariboli, G. A., "Wave Propagation in Anisotropic Elasticity," *Journal of Mathematical Analysis and Applications*, Vol. 16, Oct. 1966, pp. 108–120.

[8] Ben-Amoz, M., "The Dynamic Behavior of Tape Wound Shields Under Normal-to-Surface Impact Loads," Rept. TM SM 8156-24, Feb. 1968, Reentry Systems Dept., General Electric Co., Pa.

[9] Ewing, W. M., Jardetzky, W. S., and Press, F., *Elastic Waves in Layered Media*, McGraw-Hill, New York, 1957, pp. 76–87.

# Appendix B

Bulletin 46
(Part 4 of 5 Parts)

REPRINTED FROM

# THE SHOCK AND VIBRATION BULLETIN

AUGUST 1976

A Publication of
THE SHOCK AND VIBRATION
INFORMATION CENTER
Naval Research Laboratory, Washington, D.C.


Office of
The Director of Defense
Research and Engineering

# ISOLATION AND DAMPING

## THE MEASUREMENT OF DAMPING AND THE DETECTION OF DAMAGES IN STRUCTURES BY THE RANDOM DECREMENT TECHNIQUE

J. C. S. Yang and D. W. Caldwell
Mechanical Engineering Department
University of Maryland
College Park, Maryland

A technique called random decrement has been developed, which makes possible the computation of damping values and the detection of damage in structures when only response data is available. Damping ratios were computed using this technique for several modes of randomly excited panels, beams, and bones. These damping ratios compared satisfactorily to damping ratios which were computed from the power spectral density method. Standard randomdec signatures were established for all the structures. Damages were detected by observing the changes in the established signatures. Notches which simulated cracks were induced into two of the beams. The effects of these notches on the beams' signatures are presented.

### INTRODUCTION

When a physical structure is subjected to random forces, internal vibrations are set up within the structure as it absorbs the energy imparted to it. In some cases, the energy imparted may cause stresses which exceed the strength limitations of the structure and which may result in a failure of the structure. To prevent the failure of a structure, structural damping needs to be more thoroughly investigated. Small cracks and localized failures of the structural elements often have a significant effect on the vibration response characteristics of the structure long before they are significant enough to be visually detectable. Damping is one of the characteristics which changes. Damping is the means by which structures absorb energy and significant changes in damping are therefore very meaningful. The precise measurement of damping is therefore highly important to the economic design and reliable analysis of large structures.

Various attempts have been made to provide means for obtaining structural damping information used in the design of structures and used in the monitoring of the response to the applied forces. Although various types of apparatus and techniques are available for measuring structural responses to random vibrations, the data obtained is usually so complicated that an observer cannot readily determine when a significant change in the structural response occurs. Most of these techniques are only suitable for use under controlled laboratory conditions and are of little use for structures in service.

A simple, direct, and precise method is needed for translating the structural response time history into a form meaningful to the observer. The method chosen to examine the structure should be sensitive to changes in the natural frequencies and the damping. Power spectral density has been considered, with damping measured by the half-power point bandwidth method, but this was found to have a large measurement variance, especially when the bandwidth was small. In addition, when two modes are close, this method cannot be applied. Erroneous answers were obtained when assumed linear systems were actually nonlinear, a problem which could not be detected unless the input was also measured. The autocorrelation function was investigated as an alternative wherein damping data was obtained from the logarithmic decrement. The problem with the use of autocorrelation signatures is that the level of the curve is dependent on the intensity of the random input, and in a natural environment this can seldom be measured or controlled. If the structure is a linear system, the level changes can be compensated for by normalizing the curves, but if the structure is nonlinear (as is often the case), a different signature will be obtained with each level of excitation. Therefore, correlation functions can only be used with linear systems and by knowing the input.

Another area that needs development is the detection of crack initiation and growth. Present methods of crack detection include visual inspection and acoustic emissions. Although acoustic emissions can detect flaws in assembly line comparisons, it is highly unlikely that

under conditions of high ambient noise level such as is encountered in aircraft flight that this method can be applied. In addition, it is obvious that visual inspections are useless when cracks develop within the interior of a structural material.

In the present report a technique called "Random Decrement" is presented which makes possible the computation of damping values and the detection of damage in structures when only response data is available.

## RANDOMDEC ANALYSIS

A technique called "Random Decrement" analysis has been developed and explored initially by Cole [1], which advances the state-of-the-art in the detection of crack development and extension in structures subjected to random excitation when only response data is available. A brief summary of the method is given here.

The technique, or method of analysis, requires as input the time history of the response of a system subjected to random excitation. This time history is divided into short segments, with each segment starting with an amplitude $Y_s$. This amplitude is usually chosen to be some fraction of the standard deviation of the signal. The segments are ensemble averaged to yield the signature $\delta(\tau)$ which is a time variation of the parameter, say acceleration, strain, etc., composing the time history. The averaging process removes the effect of the random excitation and leaves a signature representing the free vibration characteristics of the structure. The averaging process also yields a signature with an initial slope of zero since the segments are divided equally into segments of positive and negative initial slopes. The method of extracting a randomdec signature is shown in Figure 1.

The degree to which the random excitation is removed from the signature depends on the number of segments averaged. Generally, good repeatability is obtained with about 500 segments. If high frequencies are being studied, say 5 KHz, a few seconds of data are needed to obtain an accurate signature.

An important part of the analysis is the filtering that is done to isolate certain frequency ranges. The time history is usually bandpass filtered; so the resulting signature shows the characteristics of the structure for that frequency bandwidth. To obtain damping, only the natural mode of interest is analyzed. This effectively reduces the response to that of a single degree of freedom system. Once the signature is obtained, damping can be found by the classical logarithmic decrement method. In addition, because of the fixed selection level, $Y_s$, it was shown that the scale and form of this signature is always the same even though the random excitation may change intensity. This independence of input intensity makes this method very attractive to use as a failure detector.

To detect flaws, a standard randomdec signature is established for the undamaged structure. Then, a flaw such as a fatigue crack will introduce an additional degree of freedom for the structure and the frequency of the flaw mode will decrease as flaw size increases. Thus when the flaw frequency couples with the modes within the analyzed bandwidth, the signature will change shape. An additional mechanism which causes distortion of the signature shape is the frictional damping caused by the interaction of the crack faces. One important characteristic of this method is that it requires no knowledge of the structural excitation other than the fact that it is random.

## EXPERIMENTAL PROCEDURE

### A. Analog Signal Recording

Three different types of structures were tested: rectangular cross-section beams, bones, and thin square panels. Table 1 contains descriptions of the specimens. Several different bones were tested. However, their first natural frequencies were at about 2,000 Hz. The digitizing rate used was too slow to obtain randomdec signatures of sufficient smoothness to measure damping for this high frequency. Therefore, a mass was mounted on top of the bones to lower their first natural frequencies.

Each beam was clamped horizontally in the center and mounted on an exciter. Accelerometers were used to pick up the input excitation and the output response of the beam to flexural vibration. An example of a mounted beam is shown in Figure 2.

Each bone was mounted vertically on a cylindrical hollowed out aluminum base which was bolted to the shaker, see Figure 3. Accelerometers were positioned inside the aluminum base and on the top end of the bone to pick up the input excitation and to sense the response of the bones to the longitudinal vibrations.

The panels were bolted with approximately clamped boundary conditions between two like reverberation chambers. The mounted panels can be seen in Figure 4. The panels were excited with a diffuse sound field with a sound pressure level of 105 dB re 0.0002 microbar. The excitation was provided by a loudspeaker located within one of the chambers. A condenser microphone was also placed within this chamber to record the signal which is representative of the random acoustical pressure variations occurring on the side of the panel. A miniature accelerometer was used to sense the response. This small, light (0.4 gram) accelerometer was utilized in order to minimize the effect of loading the structures.

A random noise generator, connected to a power amplifier was used to drive the shaker and loudspeaker. Each excitation signal used

was band-limited white noise. The white noise was low pass filtered at a cutoff frequency of about 3,500 Hz. This filtering was done to prevent the folding over of frequencies above the nyquist frequency during later digitization, and also to usefully utilize the tape recorder's full dynamic range.

Before the input and output signals were tape recorded, they were passed through Audio Frequency Spectrometers. These spectrometers were used to condition the signals and provide a rough look at the content of their frequency spectrums which were displayed by a Level Recorder. These spectrums were used to identify resonances and examine the low pass filter characteristics. Subsequently, the input and output signals were recorded on the tape recorder.

B. Digital Signal Processing and Damping Measurement

Because a digital computer cannot be used to store and operate on a continuous-time signal, it was necessary to change the analog signals into discrete-time signals. The analog to digital converter which was used had a sampling rate of 10,000 samples per second.

Power spectral density of both the input excitation and the output response was calculated. Each power spectral density resulted from 18 averaged 1024 point fast Fourier transforms. Subsequently from these results the structure's transfer function was calculated and graphically displayed. From the transfer function plot, the natural frequencies and half power bandwidths of the resonances were measured. The damping ratios were then calculated.

The same data as above was also used to calculate the randomdec signatures. Before applying the randomdec procedure to the data, the frequencies outside the narrowband time history of interest were excluded. This was accomplished by the convolution of a digital filter within the randomdec program with the data. After the narrowband data had been calculated, their mean and standard deviation were computed. The mean value was used to change the data values to have a zero mean. If this had not been done the signature would not have ended at zero as in Figure 1. A fraction of the standard deviation was used as the selected threshold level. Each time the signal values were found to cross this level, a new segment was summed to previous segments, thus calculating the randomdec signature. When the digital values of the signature were computed, a plot routine within the program displayed the curve. From this decaying sinusoidal signature, the damping ratio for various numbers of cycles were calculated by the logarithmic decrement method. The damped natural frequency was calculated from an average of the periods of oscillation.

C. Detection of Damage

To see the effect that damage might have on a structure's standard signature, notches which were assumed to simulate cracks were cut into Beams 3 and 4 as shown in Figure 5. The notches were cut with a saw blade which was approximately 0.10 cm wide. Both beams were notched 1.27 cm from the supporting fixture.

The notch in Beam 4 was cut into the full 1 inch width of the beam to a depth of 0.05 cm. Signatures from the beam's response were computed with this notch and also for five more saw cuts which extended the notch to the total depth of 0.30 cm.

Beam 3 was used to find the effect which a notch cut into a beam's side would have on it's signature. This was not expected to have quite the pronounced result on the signature as might be expected from Beam 4. However, torsional modes should be introduced by this type notch. Six damage signatures were taken for this beam from the effects of six 0.20 cm saw cuts, which made the total notch width 1.50 cm.

## RESULTS

The computer generated power spectral density and transfer function curves of the response and the excitation of a typical damped beam are shown in Figure 6 and 7. The narrowband response of one of the resonant peaks of the response was used to create the randomdec signature as shown in Figure 8. Comparisons of the transfer function and the randomdec signature damping ratio results for all the specimens are given in Table 2.

Figure 9 shows three randomdec signatures extracted from different sections of the same time history. Each of these signatures contain approximately 500 segments. These curves show the portion of the length of Beam 4's standard signature which can be considered stable enough from which to detect damage. Figures 10 and 11 show the randomdec signatures as beams 3 and 4 are damaged.

## DISCUSSION AND CONCLUSIONS

The limitations imposed by the sampling rate of the digitizer and the digital filter characteristics at low frequencies considerably reduced the number of damping ratio comparisons which were available. However, the results from Table 2 show that for most of the comparisons which were made, the damping ratios taken from the randomdec signatures and transfer function plots differed by less than a factor of two. Furthermore, the few comparisons which did differ by more than a factor of two were associated with very low values of damping.

A comparison of values of the resonant frequencies obtained from the transfer function plots with those calculated from the periods of the randomdec signatures show that all but one differed by less than 6 percent. Considering that the randomdec signatures were calculated from only response data while it was necessary to also use the excitation data for the calculation of the transfer function, these results are very good. This is especially true for the panels since the excitation spectrum was very non-uniform.

Figure 9 shows the results of extracting three randomdec signatures from different portions of the same narrowband time history. It can be seen that for approximately the first 8 milliseconds all the signatures are almost identical. This portion of the signature can be used as a standard from which damage can be detected.

Figures 10 and 11 show the signatures resulting from the damaged beams. Both figures show that the effects of the saw cut in each beam had a significant effect on the standard signatures.

The satisfactory results obtained from the experimental comparisons indicate that the randomdec technique is a valid method of measuring damping. Also, the randomdec signatures of the damaged beams demonstrate its ability to detect the induced flaws.

ACKNOWLEDGEMENT

This work was jointly supported by the Minta Martin Fund, College of Engineering and the Computer Science Center, University of Maryland.

REFERENCE

Cole, Henry A., Jr., "On-Line Failure Detection and Damping Measurement of Aerospace Structures by Random Decrement Signatures," NASA CR 2205, Mar. 1973.

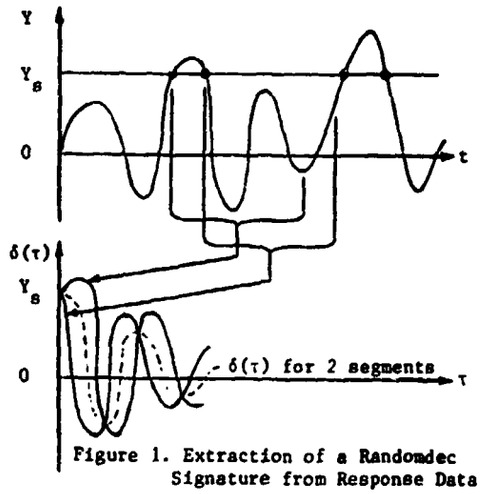


Figure 1. Extraction of a Randomdec Signature from Response Data

Figure 2. Mounted Beam on Shaker

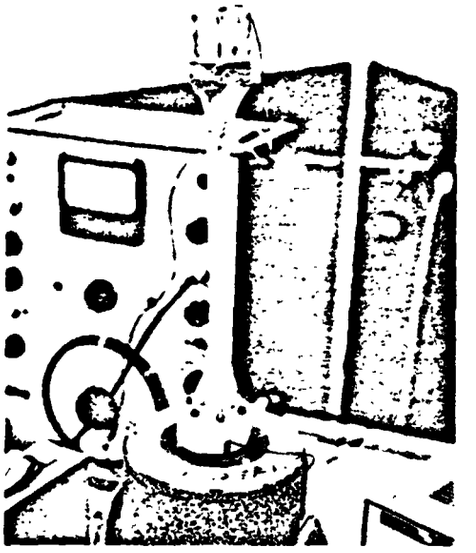

Figure 3. Mounted Bone on Shaker

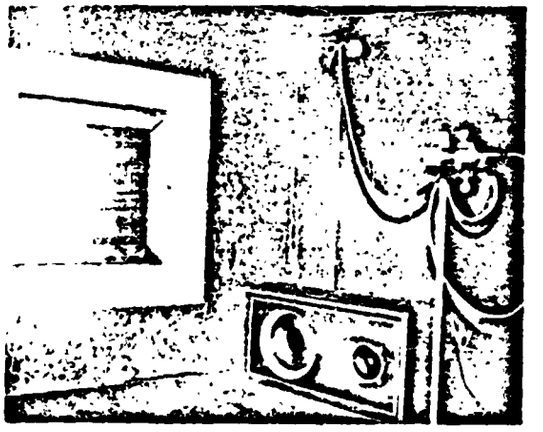

Figure 4. Mounted Panel in Chamber

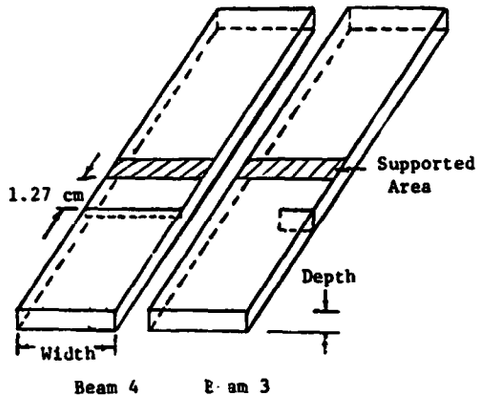


Figure 5. Notched Beams

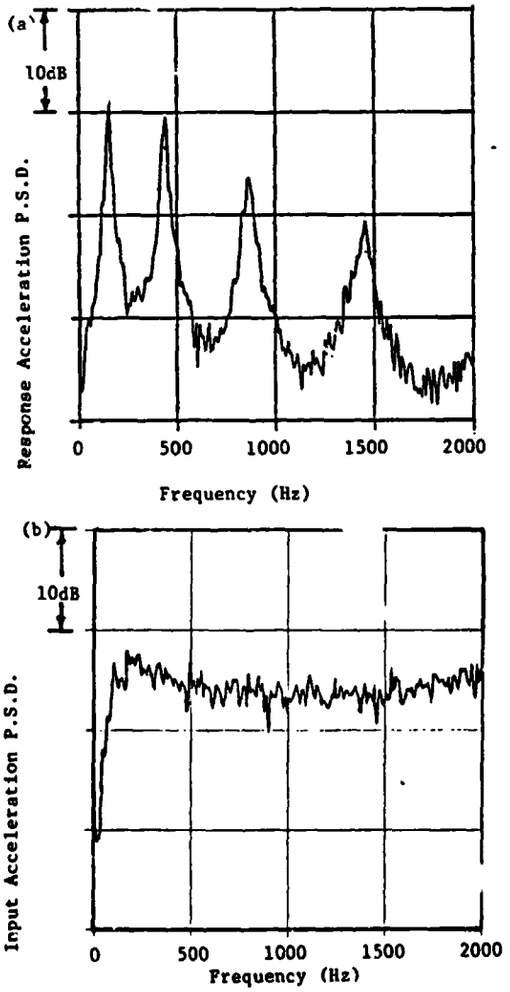


Figure 6. Typical Power Spectral Density Plots
(a) Response (b) Input

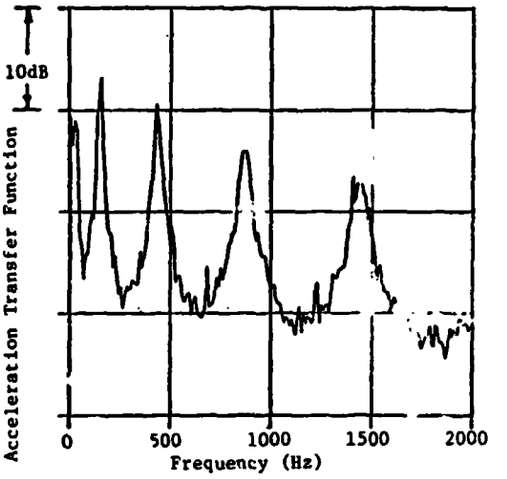


Figure 7. Typical Transfer Function Plot

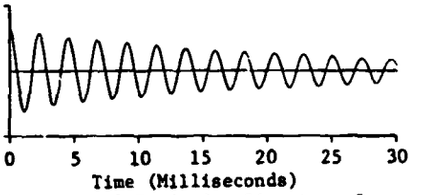


Figure 8. Typical Randomdec Signature from Narrowband Response Time History

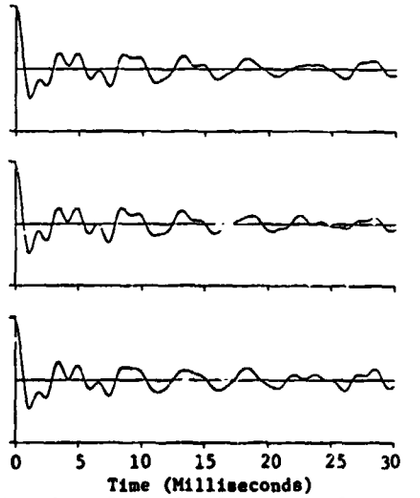


Figure 9. Three Randomdec Signatures from Different Records of Undamaged Beam 4 Response

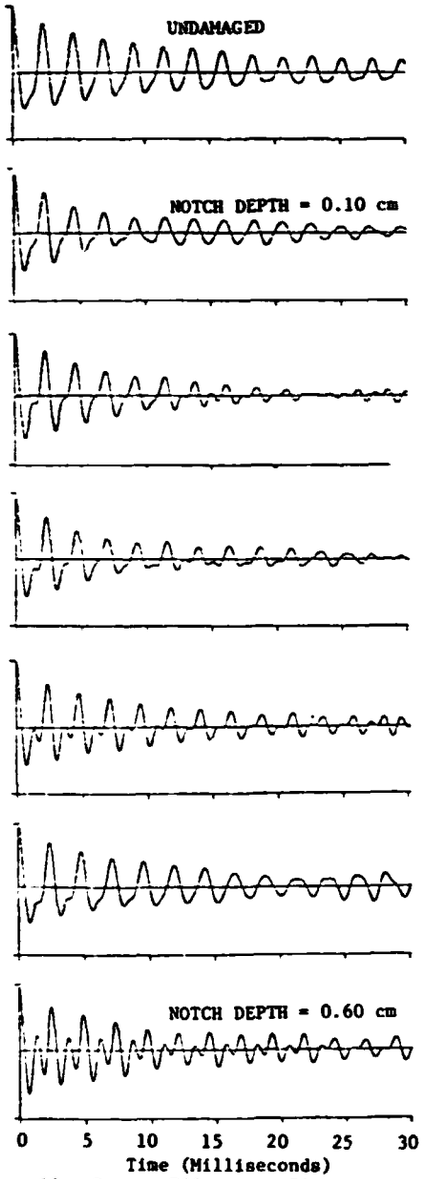


Figure 10. Damage Effects on Signature of Beam 3 Broadband Response

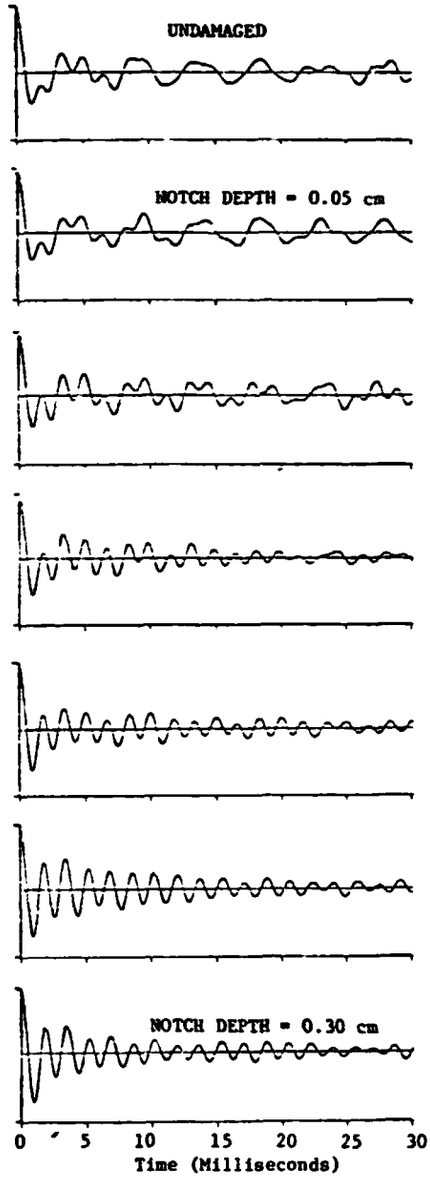


Figure 11. Damage Effects on Signature of Beam 4 Broadband Response

TABLE 1. Descriptions of Beams and Panels

Beams

| Number | Material | Length (cm) | Thickness (cm) | Width (cm) |
|---|---|---|---|---|
| 1 | Aluminum | 42.5 | 0.124 | 2.54 |
| 2 | Aluminum | 42.5 | 0.325 | 2.54 |
| 3 | Plexiglass | 42.5 | 0.318 | 2.54 |
| 4 | Plexiglass | 42.5 | 0.432 | 2.54 |
| 5 | Glass | 34.9 | 0.635 | 2.54 |
| 6 | Glass | 37.5 | 0.635 | 2.54 |

Panels*

| Number | Material | Thickness (cm) | Lamina Lay Up (degrees) |
|---|---|---|---|
| 1 | Aluminum | 0.084 | Homogenous |
| 2 | Hercules 3501/ AS Graphite/ Epoxy | 0.099 | 0/90/0/90/90/0/90/0 |
| 3 | Hercules 3501/ AS Graphite/ Epoxy | 0.112 | 45/-45/45/-45/-45/45/-45/45 |
| 4 | Hercules 3501/ AS | 0.109 | 22.5/-22.5/22.5/-22.5/-22.5/ 22.5/-22.5/22.5 |

*All panels are 30.5 cm x 30.5 cm

TABLE 2. Consolidation of Results

| Specimen | Cut-Off Freqs. (Hz) | Transfer f(Hz) | Function $\zeta$ | Randomdec $f_d$(Hz) | Signature $\zeta_{Avg}$ | Comparison $\frac{f}{f_d}$ | $\frac{\zeta}{\zeta_{Avg}}$ |
|---|---|---|---|---|---|---|---|
| Beam 1 | 350-600 | 455 | .025 | 458 | .014 | .994 | 1.79 |
| Beam 1 | 750-1050 | 901 | .013 | 896 | .013 | 1.004 | 1.00 |
| Beam 2 | 250-550 | 350 | .026 | 387 | .003 | .982 | 8.67 |
| Beam 2 | 800-1300 | 1060 | .008 | 1076 | .001 | .985 | 8.00 |
| Beam 3 | 300-650 | 433 | .032 | 441 | .016 | .982 | 2.00 |
| Beam 3 | 650-1100 | 868 | .033 | 879 | .022 | .987 | 1.50 |
| Beam 4 | 400-900 | 613 | .022 | 622 | .029 | .985 | .76 |
| Beam 4 | 900-1500 | 1225 | .017 | 1225 | .020 | 1.000 | .85 |
| Beam 5 | 900-1300 | 1065 | .019 | 1099 | .001 | .969 | 19.00 |
| Beam 6 | 800-1100 | 868 | .004 | 909 | .002 | .955 | 2.00 |
| Bone 1 | 500-1500 | 985 | .019 | 1039 | .019 | .948 | 1.00 |
| Panel 1 | 135-190 | 166 | .051 | 164 | .036 | 1.012 | 1.42 |
| Panel 2 | 140-190 | 175 | .017 | 173 | .019 | 1.011 | .89 |
| Panel 3 | 190-250 | 224 | .040 | 193 | .042 | 1.160 | .95 |
| Panel 4 | 190-270 | 215 | .061 | 200 | .039 | 1.075 | 1.56 |

# Appendix C

# RESPONSE OF PLATES TO RANDOM PRESSURE LOADING FROM A TURBULENT BOUNDARY LAYER

William T. Messick*
Jackson C. S. Yang**

The study of structural response to turbulent boundary layers is very important for determining fatigue life and noise transmission to the interior of aerospace vehicles. To gain insight into the problem, the response of clamped plates to a cross spectral density function representing the pressure loading from an attached turbulent flow is studied. As a preliminary study to determining the response of composite material plates, an isotropic plate is modeled with finite elements and its response is compared to theoretical and experimental results. The modal frequency and random response rigid format number 11 of NASTRAN was used for determining the natural frequencies, nodal patterns, and displacement power spectral densities.

The plate that was modeled has clamped edges, is made of steel of density 0.27 pounds per cubic inch and measures 4.0 inches in the flow direction by 2.75 inches wide by 0.015 inches thick. A grid was chosen that has nodes at the quarter and mid points of the plate for comparison with references 1 and 2. To keep computer running time to a minimum, a relatively coarse 8x8 grid was chosen. The CQUAD2 element with the coupled mass (COUPMASS) option was used for the finite element model. Constraining the membrane degrees of freedom, the rotations about the normal, and the clamped edges yields a problem with 147 degrees of freedom. The eigenvalues in the frequency range of 0 to 3000 cps were determined using rigid format 3 in NASTRAN and compared with those calculated from:

$$f_i = \frac{\lambda_i}{2\pi}\left(\frac{Eh^3}{12(1-\nu^2)\rho a^4}\right)^{1/2} \qquad (1)$$

where $\nu$ is Poisson's ratio

$E$ is the modulus

$\rho$ is the density per unit area

$h$ is the plate thickness

$a$ is the plate width

and $\lambda_i$ is the characteristic value of the $i^{th}$ mode and a function of the plate aspect ratio.

* Mechanical Engineer, Naval Ordnance Laboratory, White Oak, Md.
**Professor, Mechanical Engineering Department, University of Maryland

The computed NASTRAN values and the error associated with each mode based on the characteristic values tabulated in reference 3 are shown in Table 1. The agreement is very good for the coarse mesh.

| Mode Number (m-n) | NASTRAN Natural Frequencies for a Clamped 8x8 Grid (cps) | Error |
|---|---|---|
| 1-1 | 542.9 | 0.1% |
| 2-1 | 856.0 | .03% |
| 1-2 | 1330.0 | 1.1% |
| 3-1 | 1404.2 | 1.3% |
| 2-2 | 1611.5 | 0.3% |
| 3-2 | 2087.2 | -0.7% |
| 4-1 | 2210.4 | 5.0% |
| 1-3 | 2551.5 | 2.3% |
| 2-3 | 2791.3 | 0.7% |
| 4-2 | 2798.2 | 1.5% |

Table 1 - Natural Frequencies Obtained From NASTRAN 8x8 Grid for a Clamped Plate

The pressure fluctuations that occur on a flat surface due to a turbulent boundary layer may be expressed in terms of random variables which are spatially and temporarily correlated. For homogeneous turbulence, the cross spectral density depends only on the separation distance of two points. Furthermore, the cross correlation coefficient is separable in terms of streamwise and cross flow directions so that the cross spectral density is expressed in the form:

$$\frac{S_p(\xi_1,\xi_2,\omega)}{S_p(\omega)} = |\rho_p(\xi_1,0,\omega)|\,|\rho_p(0,\xi_2,\omega)|\,(\cos\frac{\omega\xi_1}{U_c} - i\sin\frac{\omega\xi_1}{U_c}) \qquad (2)$$

where $\xi_1$ and $\xi_2$ are the streamwise and cross flow separation, respectively, of two points, $\omega$ is the circular frequency, and $U_c$ is the narrow band convection velocity. $|\rho_p(\xi_1,0,\omega)|$ and $|\rho_p(0,\xi_2,\omega)|$ are correlations

coefficients for the streamwise and cross-flow directions, respectively, which depend on the type of flow. This is the general form of the function that was input to NASTRAN using the RANDPS bulk data card. The general form of the RANDPS input is

$$g(\omega)(X + iY) \tag{3}$$

where X and Y are constants. However, for the function of interest, X and Y should be functions of frequency. As a result, a separate set of RANDPS cards had to be generated for each frequency and a separate computer run made for each one.

For the subsonic flow case, the cross correlation coefficients have been shown by Bull (reference 4) to be

$$\begin{aligned} \rho_p(\xi_1,0,\omega) &= e^{-0.1\ \omega|\xi_1|/U_c} \quad \text{if} \quad \omega\delta^*/U_c \geq 0.37 \\ &= e^{-.037|\xi_1|/\delta^*} \quad \text{if} \quad \omega\delta^*/U_c < 0.37 \end{aligned} \tag{4}$$

$$\begin{aligned} \rho_p(0,\xi_2,\omega) &= e^{-.715\ \omega|\xi_2|/U_c} \quad \text{if} \quad |\xi_2| \geq -\delta^*\left[9.1 \log\left(\frac{\omega\delta^*}{U_c}\right) + 5.45\right] = C \\ &= 0.28 + 0.72\ e^{-0.547|\xi_2|/\delta^*} \quad \text{if} \quad |\xi_2| < C \end{aligned} \tag{5}$$

where $U_c = (0.59 + 0.3\ e^{-0.89\ \omega\delta^*/U_\infty})$

$U_\infty$ is the free stream velocity

and $\delta^*$ is the displacement boundary thickness

Using the boundary layer thickness of 0.179 inches for the Mach number 0.3 case (reference 4) the cross spectral density values were evaluated for 9 frequencies in the 0-3000 cps range. Only the modes in this frequency range were used for the modal solution. A structural damping coefficient of 0.009 was used in order to compare the results with the modal analysis in reference 1. The NASTRAN results, the modal analysis results of reference 1, and the experimental results of reference 2 are shown plotted in Figures 1 and 2 for the displacement power spectral density of the panel quarter point and mid point, respectively. The running time on the University of Maryland UNIVAC 1108 using NASTRAN level 15.1.0 was 463 CPU seconds for the eigenvalue analysis and the displacement power spectral density at one frequency. With a checkpointed tape of the eigenvalue analysis, each succeeding run time was 149 seconds per frequency.

The agreement of the NASTRAN results with the modal analysis of reference 1 is excellent considering the relatively coarse mesh. There is a discrepancy at the panel midpoint for the ninth natural frequency but the difference is less than an order of magnitude. The agreement with the experimental values is also very good. It appears that with an additional number of NASTRAN calculations, the root mean square response of the panel can be adequately predicted. However, although the displacement power spectral density at a particular frequency may be obtained at a reasonable cost, the generation of a sufficient number of points for the root mean square displacement becomes an expensive proposition. To help decrease the running time it would be advantageous to allow the real and imaginary parts to be separate functions of frequency and let these functions be evaluated at a number of frequencies for one computer run.

Future studies will investigate the effect of filament orientation on the random response of composite plates. An orthotropic constitutive matrix will be input and a finer mesh used for the NASTRAN analysis.

## ACKNOWLEDGEMENT

The study was supported by the Aeronautical Structures Branch, Ames Research Center, National Aeronautics and Space Administration, under Grant NGR 21-002-350. This support is gratefully acknowledged.

## REFERENCES

1. Chyu, W. J. and Au-Yang, M. K., "Random Response of Rectangular Panels to the Pressure Field Beneath a Turbulent Boundary Layer in Subsonic Flow," NASA TN-D-6970, October 1972

2. Wilby, J. F., "The Response of Simple Panels to Turbulent Boundary Layer Excitation," AFDL-TR-67-70, October 1967

3. Leissa, A. W., "Vibration of Plates," NASA SP-160, 1969

4. Bull, M. K., "Wall-Pressure Fluctuations Associated with Subsonic Turbulent Boundary Layer Flow," J. of Fluid Mech., Vol. 28, pt. 4, pp. 719, 1967

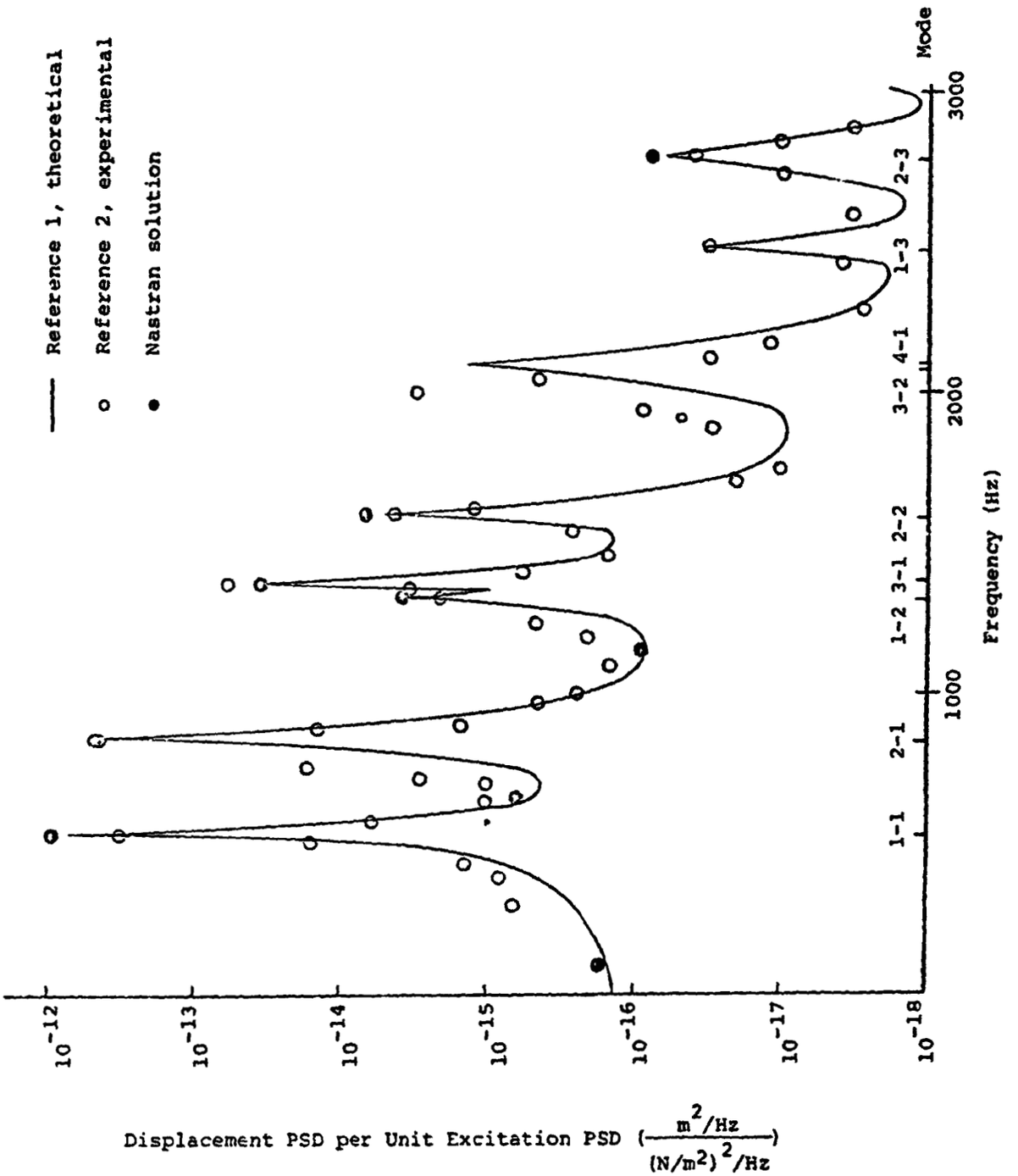


Figure 1 - Displacement PSD Response at Panel Quarter Point for M=0.3

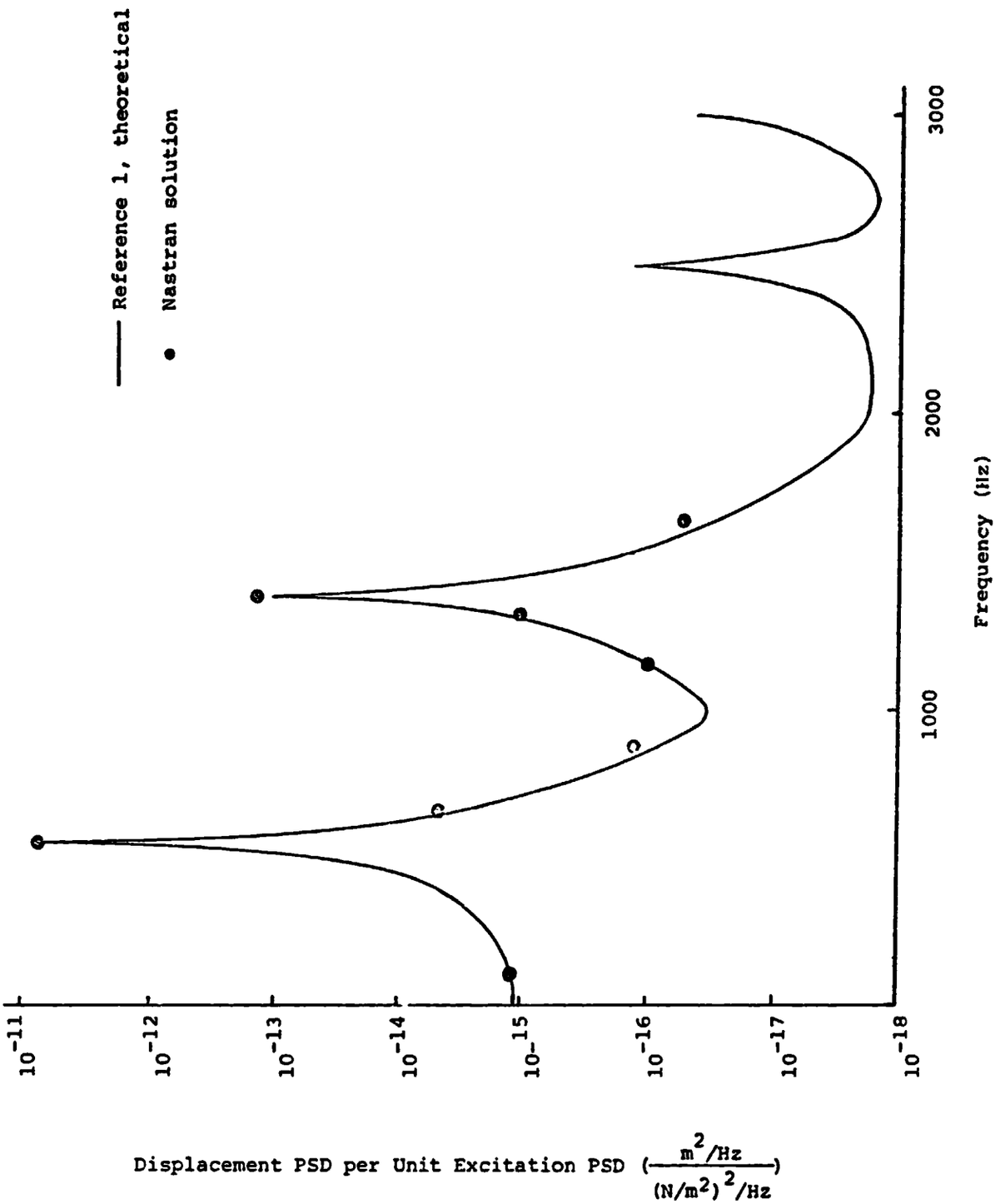


Figure 2 - Displacement PSD Response at Panel Midpoint for M=0.3

# Appendix D

# THE DESIGN OF SMALL REVERBERATION CHAMBERS FOR TRANSMISSION LOSS MEASUREMENT

CHUNG Y. TSUI, CARL R. VOORHEES* and JACKSON C. S. YANG

*Department of Mechanical Engineering, University of Maryland, College Park, Maryland 20742 (USA)*

*SUMMARY*

*This paper describes the design, construction and performance evaluation of a small test facility for transmission loss measurement. The low-cost test facility—in the form of a twin pentagonal parallelepiped—is made of laminates of masonite, fibreglass, and plywood and is particularly adaptable for transmission loss tests of small panels.*

## INTRODUCTION

The accurate assessment of the sound insulation properties of panels and partitions is an important area in acoustics, as is indicated by past research. This aspect of research took on a new importance recently with the revelation that a quiet environment is imperative for healthy living and efficient working. In order to protect privacy, as well as prevent hearing damage to the public, legislation and ordinances against excessive noise exposure have been promoted by all levels of government.

Sound insulation data are essential to architects and noise control specialists in their planning for an environment with comfortable noise levels. Economic considerations dictate that this desirable environment be designed into new buildings and structures, rather than be treated later as an 'add on' feature. These data are also required when remedial modifications are made to existing designs.

The sound insulation property is most commonly obtained by the two-room method, especially for panels and partitions. In this method, the test specimen is placed in the common wall between the source room and the receiving room, and the noise reduction between the rooms is recorded experimentally. The result is expressed by the transmission loss, TL, defined by:

$$TL = 10\log_{10}(1/\tau) \qquad (1)$$

* Present address: Applied Acoustics Section, National Bureau of Standards, Washington, DC 20234 (USA).



*Applied Acoustics* (9) (1976)—
Printed in Great Britain

where $\tau$ is the ratio of the transmitted energy to the incident energy. Measurement procedures and precautions can be found in recommended standards such as ASTM E90,[1] published by the American Society for Testing and Materials.

According to the standard, the transmission loss is given by:

$$TL = NR + 10\log_{10} S - 10\log_{10} A_2 \quad (2)$$

where NR is the noise reduction between the source room and the receiving room, $S$ is the area of the sound transmitting surface of the test specimen and $A_2$ is the total absorption of the receiving room expressed in units consistent with $S$.

The derivation of this equation is based on many assumptions. The most important is that the sound field in the rooms be sufficiently diffused. This is not surprising as, in the design of rooms for measurement, the attainment of a diffused sound field has caused the most concern. The design of small rooms is no exception, as is reported in this paper.

Many methods have been devised in order to achieve a relatively high degree of diffusivity. Some of the more important are outlined below.

*Rotating reflector*

A motorised rotating reflector placed in a room effectively creates a variable boundary of the room which results in oscillation and the appearance and disappearance of modal patterns for a constant sound source. The circulation of the air in the room also breaks up the modal patterns to achieve a better diffused sound field.

*Reflecting surfaces*

Highly reflective surfaces are added to the rooms by hanging objects from the ceiling. This increases the sound reflecting area for a given room volume without appreciably increasing the room absorption, thus enhancing sound diffusion through multiple reflections.

*Non-parallel walls*

This enables the sound waves in a room to impinge against the walls more randomly at various angles of incidence. Given a constant volume, the total number of normal modes for an irregularly shaped room is very close to that for a room with parallel walls. However, the degeneracy of modes due to the overlap of modal patterns in an irregularly shaped room is much less and, consequently, a better diffused sound field is obtained.

*Multiple frequency sound source*

A source such as a warble tone or a third-octave band noise has energy over a wider frequency range than a pure tone. This source is capable of generating a series of modal patterns, each pertaining to a narrowly grouped frequency band. The application of such a source in the measurement of transmission loss is an

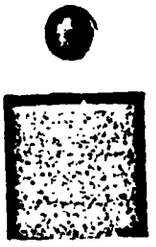

operational practice and is actually required in the ASTM E90 procedures. It is, however, unrelated to the design and construction of the chambers.

There exist many rooms[2-6] which have the desirable sound diffusion characteristic. These rooms are very reverberant and are commonly referred to as reverberation chambers. Located at various acoustical laboratories associated with research organisations, universities and manufacturers of acoustical materials, these rooms are also used for the measurement of power outputs of sound sources and sound absorption coefficients. For the measurement of transmission loss, however, two adjacent reverberation chambers are required.

Due to the fact that acoustical characteristics, including transmission loss at frequencies as low as 100 Hz and under, are required for full-sized building components such as doors and wall assemblies, these rooms are generally large, ranging in size from 1000 to over 10,000 $ft^3$. The walls are generally made of massive concrete, 1 to 3 ft thick. There are inherent drawbacks with these large rooms. The first of these drawbacks is one of economics. The building and equipping of the rooms is costly and generally regarded as a major investment for a good acoustical laboratory. The second and more critical drawback is the acoustical permanence of the rooms. Because of their large size, the acoustical characteristics of the rooms are difficult to change. Therefore, for a given test facility, it is nearly impossible to assess the effects of the many important parameters which would influence the results of the measurement. In the same way, it would serve no useful purpose to reconcile for measurement discrepancies results from non-identical test facilities, even though the method of measurement and the specimen were identical. A large test facility is generally unfit for testing specimens which are small compared with full-sized building partitions or doors. This inadequacy is particularly significant for transmission loss tests as the sound energy must be transmitted from the source room to the receiving room through a tunnel formed by the thick walls. The specimen will not be exposed to sound through a wide range of angles of incidence. Errors in measurement will also be larger as the size of the specimen becomes smaller due to the increasing proportion of transmitted energy through the common wall.

Small test chambers are justified because they avoid the above drawbacks. It is possible to quickly and inexpensively change any room parameter in order to investigate its influence on test results. By eliminating the tunnel effect, these chambers are also more adaptable for testing small panels and components. The latter advantage becomes even more attractive in aerospace applications as most of the panels and components are inherently small. In some cases, it is required to test new materials for their acoustical properties when only a small sample of the material is available. The drawback of small test chambers lies mainly in their high cut-off frequency, which means that it is not possible to obtain reliable sound insulation information in the low frequency range. Whether this constitutes an unacceptable handicap is dependent on the intended application and must be resolved before the measurement is undertaken.

## DESIGN AND CONSTRUCTION OF TEST FACILITY

The test facility to be constructed was designed to yield reliable transmission loss data for small panels. The internal dimension of the rooms was limited to between 3 and 4 ft at an edge. It was decided, because of the size, that it was not feasible to have motorised rotating reflectors, and that a pair of twin chambers made of plywood and masonite laminated boards would be the easiest type of facility to construct. To

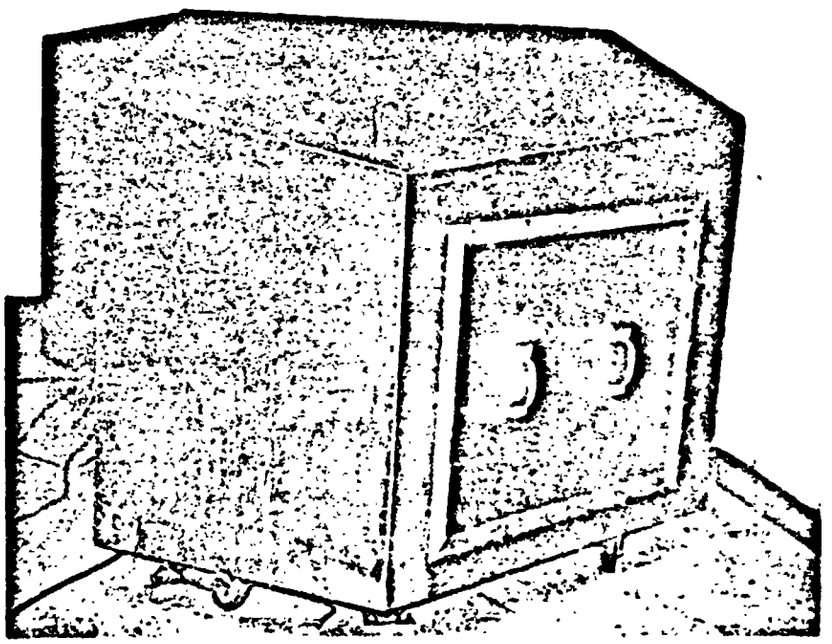

Fig. 1. Twin reverberation chambers for transmission loss measurement.

increase sound diffusivity, non-parallel vertical walls in the form of a pentagon with an inclined roof and a level floor were adopted. It can readily be appreciated that in choosing this particularly simple configuration, correct dimensions of the wall boards, especially at the edges, can accurately be obtained through geometrical development, thus ensuring good acoustical seals. The shape of the twin parallelepiped facility, which is shown in Fig. 1, very closely resembled those at the Kobayasi Institute in Japan.[2] A schematic view of the test chambers is given in Fig. 2.

The common wall and the floor of the rooms were made of 1·75 in laminate of two 0·75 in plywood and one 0·25 in masonite boards. The other walls and the ceiling of the rooms were made of 1 in laminate of plywood and masonite, reinforced by a wooden grid of one-by-three ribs. A 0·25 in outer masonite sheet enclosed a 3 in lining of Owen-Corning 703 Fiberglas insulation. The laminated boards were assembled and all joints were glued and fastened with screws. Acoustical sealant was applied along all edges to ensure a tight seal against noise leakage.

The 22 $in^2$ × 4·5 in frame for mounting the test panel was constructed of hardwood pieces of 3 in × 4·5 in cross-section, was rigidly attached to the receiving room and protruded through an opening in the common wall (Fig. 2). A panel size of 16 in × 16 in could be fitted into the frame and clamped securely between 2 in steel facing plates, leaving an exposed area of 12 in × 12 in.

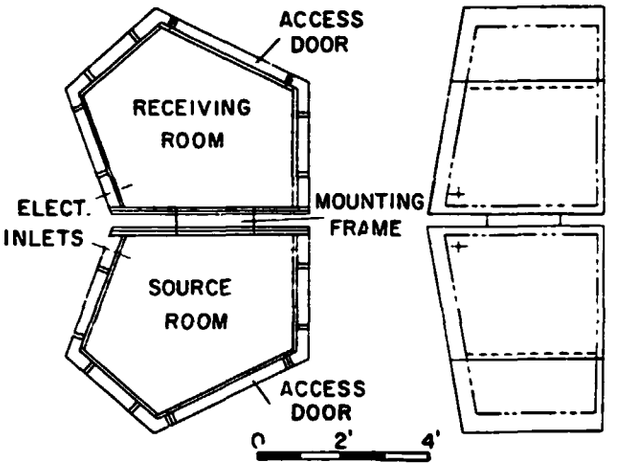


Fig. 2. Schematic view of the twin reverberation chambers.

To facilitate access to the test panel and the measuring equipment, a 28 in × 34 in opening was made in a rear wall of each room (Fig. 2). The opening was closed by a door of the same construction as the wall and was sealed on the inner and outer edges with a 2 in aluminium flange and rubber gasket. Electrical wiring was fed through a side wall at a location near the ceiling and the common wall (Fig. 2). The small hole in the wall was subsequently plugged with cork and acoustical sealant.

A microphone traversing mechanism was designed to carry a microphone continuously over a linear path. When activated, the unit traversed at approximately 8 in/min and automatically reversed direction at the end of each crossing. The traversing guide could be mounted at two different ceiling positions in each room

with the microphone suspended at two heights to provide four different microphone paths (Fig. 3).

In connecting the twin chambers, the mounting frame was pushed into a similar opening in the common wall of the source room and pressed against a resilient stop at the inner side. The common spacing between the rooms was about 1 in and was filled with Owen-Corning 703 Fiberglas. The small gaps between the common walls and the mounting frame were also filled with acoustical sealant. This arrangement allowed no rigid connections, thus discouraging flanking and structural transmission between the two rooms.

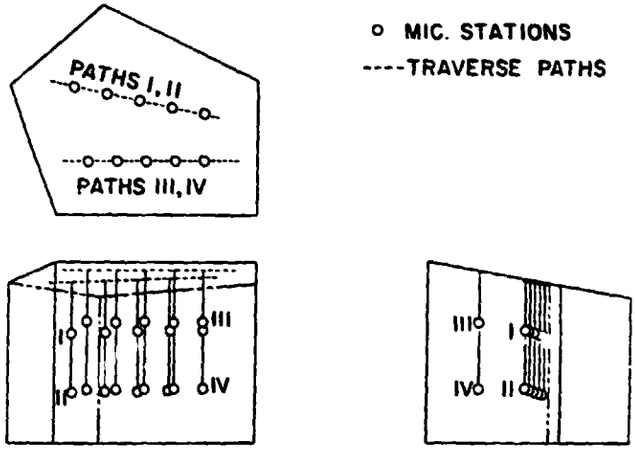


Fig. 3. Microphone traverse paths and measurement stations.

The completed test facility consisted of a pair of twin chambers each having a volume of 48 $ft^3$ and a surface area of 83 $ft^2$.

## TEST FACILITY PERFORMANCE EVALUATION

Several tests were conducted to evaluate the performance of the facility. These tests established the lower frequency limit and the minimum sound pressure levels in the receiving room in order to yield valid transmission loss data for the specimens tested.

*Diffusivity measurement*

At various third-octave excitations, sound pressure levels along microphone traverses were recorded in order to examine the spatial variations. Two representative sets of results over four different traversing paths are shown in Fig. 4.

These results were obtained at centre frequencies of 315 Hz and 400 Hz. Sound pressure level variations along the same paths at other centre frequencies were found to be less significant for excitations higher than 400 Hz and were more significant for excitations with centre frequencies lower than 315 Hz. These results indicate that the lower cut-off frequency for the test facility is at about 400 Hz. This value is slightly lower than the derived 500 Hz, according to an equation in ASTM E90, to assure the achievement of an adequate number of room modes.

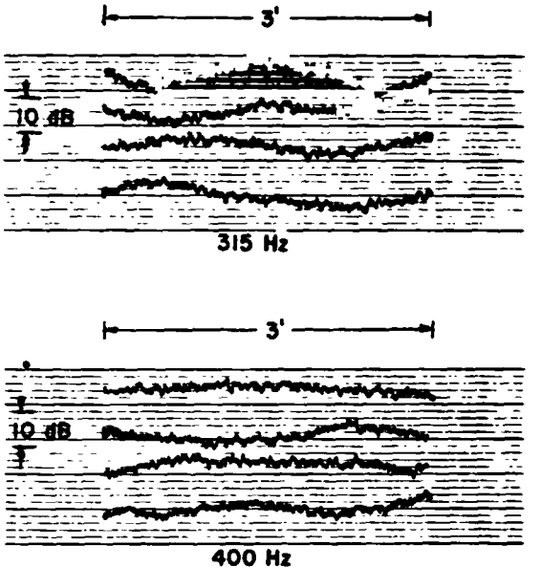


Fig. 4. Sound pressure level variations at 315 Hz and 400 Hz.

*Reverberation time measurement*

The reverberation times of each room were determined from the decay curves (Fig. 5) of third-octave excitations ranging from 400 Hz to 4000 Hz. ASTM C423 requirements[7] were followed. In addition, the absorption coefficients of the walls of the rooms were obtained from the Sabine equation.[1] The calculated results are shown in Table 1. Each number in the Table is the average of 20 microphone positions shown in Fig. 3. In most cases (*see* Table 1) the absorption coefficients meet the ASTM E90 recommendation of 0·06 for good sound reflections. The constant decay slope of the curves in Fig. 5 which were obtained at different stations also indicates that a good diffused sound field exists at 400 Hz.

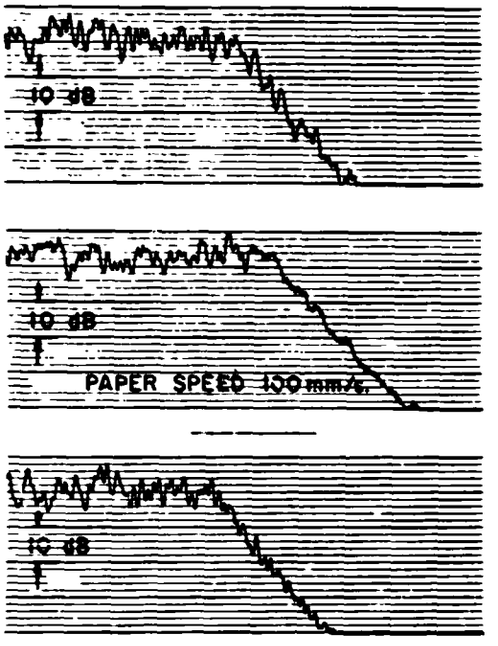


Fig. 5. Decay curves at 400 Hz.

*Field transmission loss measurement*

Field transmission loss measurement provides the noise reduction between two adjacent rooms separated by a common wall. This concept was applied to the present case in the establishment of the minimum sound pressure levels in the receiving room over the background noise levels surrounding the test facility for reliable transmission loss measurements. In this case, the two adjacent rooms were the receiving room and the laboratory which housed the test facility; the common wall

TABLE 1
REVERBERATION TIMES AND ABSORPTION COEFFICIENTS OF THE TEST FACILITY

| *Third-octave centre freq. (Hz)* | 400 | 500 | 630 | 800 | 1000 | 1250 | 1600 | 2000 | 2500 | 3150 | 4000 |
|---|---|---|---|---|---|---|---|---|---|---|---|
| $T_{60}$ Source rooms | 0·450 | 0·550 | 0·510 | 0·470 | 0·450 | 0·400 | 0·470 | 0·450 | 0·460 | 0·430 | 0·460 |
| $T_{60}$ Receiving rooms | 0·430 | 0·484 | 0·503 | 0·503 | 0·482 | 0·486 | 0·481 | 0·448 | 0·419 | 0·404 | 0·408 |
| $\alpha$ Source room | 0·061 | 0·050 | 0·054 | 0·058 | 0·061 | 0·068 | 0·058 | 0·061 | 0·059 | 0·063 | 0·059 |
| $\alpha$ Receiving room | 0·064 | 0·056 | 0·054 | 0·054 | 0·057 | 0·056 | 0·057 | 0·061 | 0·065 | 0·068 | 0·067 |

was the set of walls, ceiling, and floor of the receiving room. In the measurement, ASTM E336 requirements[8] were followed and the results are given in Table 2. Therefore, an ambient noise level of 40 dB in the laboratory will result in a background noise level of 3 dB in the receiving room; for reliable transmission loss data, the recorded sound pressure level should be at least 10 dB higher or above 13 dB in the receiving room.

TABLE 2
FIELD TRANSMISSION LOSS OF THE RECEIVING ROOM WALLS

| *Octave centre freq. (Hz)* | 250 | 500 | 1000 | 2000 | 4000 |
|---|---|---|---|---|---|
| $\bar{\alpha}$, Laboratory | 0·18 | 0·25 | 0·30 | 0·27 | 0·26 |
| SPL Laboratory, dB | 80 | 80 | 80 | 75 | 75 |
| $\bar{\alpha}$, Receiving room | 0·052 | 0·052 | 0·063 | 0·063 | 0·062 |
| SPL, Receiving room, dB | 58 | 57 | 57 | 47 | 43 |
| Field transmission loss, dB | 34 | 35 | 34 | 39 | 43 |

*Flanking transmission loss measurement*

This is a measurement of the transmission loss of a panel of very high sound insulation resistance. The result indicates the degree of flanking transmission through paths other than the test panel. For a panel under actual test, the transmission loss measurement should then be somewhat less in order to ensure that most of the sound energy is transmitted through the panel. The flanking transmission measurement then established an upper limit for valid transmission

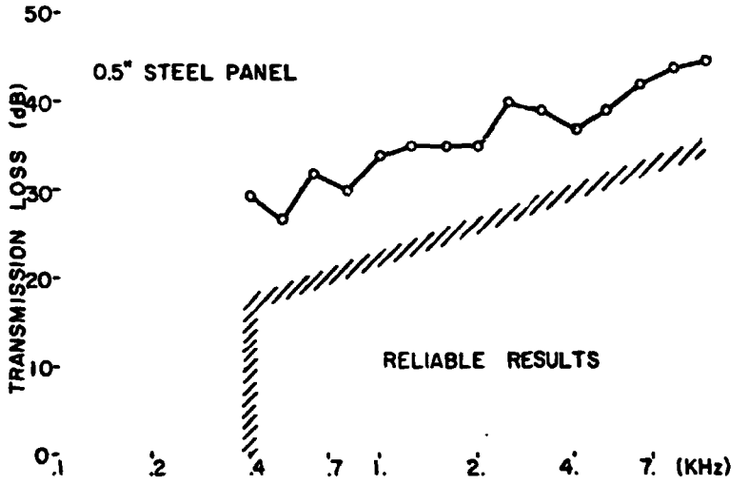


Fig 6 Flanking transmission loss of test facility and region of reliable measurement results.

measurement results for the test facility. In this test, a 0·5 in steel panel was used and the results are given in Fig. 6.

Based on the evaluation tests, a region of reliable transmission loss measurements for the test facility can be obtained. This region is bounded by hatched lines (Fig. 6) on the left at 400 Hz and from above by a line approximately parallel to the flanking transmission loss curve but set arbitrarily 10 dB below it. Transmission loss measurements for a panel within this region are valid and reliable.

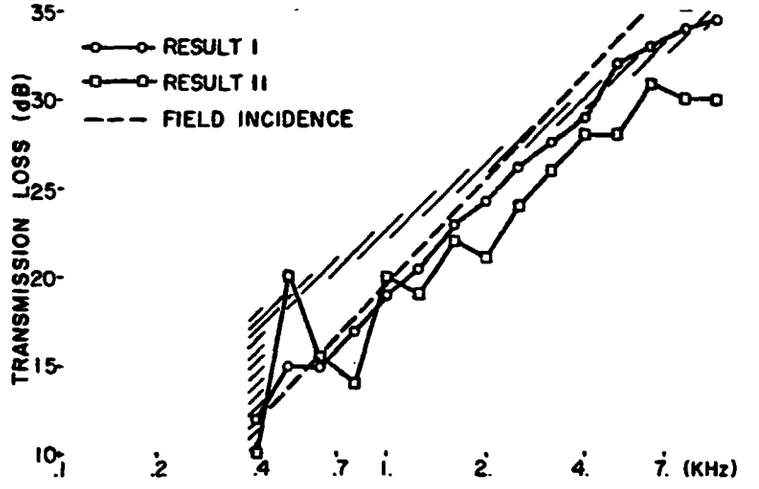


Fig. 7. Results of transmission loss measurements by the test facility.

The test facility was used to obtain transmission loss data for two 16 in × 16 in panels with the results shown in Fig. 7. Result I refers to a 0·033 in aluminium panel of surface density of 0·46 lb/ft$^2$. This curve is compared to a field incidence curve defined by:[9]

$$(TL)_{\text{field incidence}} = (TL)_0 - 5\,\text{dB} \tag{3}$$

where $(TL)_0$ is the transmission loss calculated from the normal incidence limp-wall law. The result exhibits the well-known mass-controlled behaviour in the frequency range of 400 to 10,000 Hz. Result II refers to a 0·039 in graphite epoxy composite panel with 45° fibre orientation and surface density of 0·36 lb/ft$^2$. The panel exhibits stiffness-controlled effects in the frequency range 400 to 1000 Hz due to its high modulus of elasticity but reverts to mass-controlled behaviour in the frequency range 1000 to 10,000 Hz. Due to the smaller surface density, the transmission loss for the composite panel is some 2 dB lower than that for the aluminium panel. If the thickness of the aluminium panel were decreased to 0·026 in, the surface density would be comparable with that of the composite panel and the transmission loss for the two panels would virtually be equal.

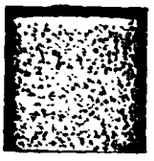

In summary, it is possible to conclude, based on results obtained, that the 0·039 in composite panel tested is as effective a sound barrier as a 0·026 in aluminium panel in the frequency range of approximately 1000 Hz to 10,000 Hz. When subjected to a random acoustical loading, a composite panel appears to react similarly to those made of more conventional materials, notably in the mass-controlled frequency range. Because of this, the advantage of the light weight of the material is offset by higher noise transmission.

## ACKNOWLEDGEMENT

The authors gratefully acknowledge the support of the NASA Ames Research Center through Research Grant NRG 21-002-350.

## REFERENCES

1. ASTM E90-70, Laboratory Measurement of Airborne Sound Transmission Loss of Building Partitions, American Society for Testing and Materials, Philadelphia.
2. K. SATO and M. KOYASU, On the new reverberation chamber with non-parallel walls, *J. Physical Soc. Japan*, **14** (1959) pp. 670–7.
3. D. R. MCAULIFFE, Design and performance of a new reverberation room at Armour Research Foundation, Chicago, Ill., *J. Acoust. Soc. Am.*, **29** (1957) pp. 1270–3.
4. R. L. RICHARDS, New airborne sound transmission loss measuring facility at Riverbank, *J. Acoust Soc. Am.*, **30** (1958) pp. 999–1004.
5. E. BROSIO, Measurement of the sound insulation by random and by normal incidence of sound. *Acoustica*, **10** (1960) pp. 173–5.
6. F. INGERSLER, O. J. PEDERSON and P. K. MOLLER, New rooms for acoustic measurements at the Danish Technical University, *Acoustica*, **19** (1967) pp. 185–97.
7. ASTM C423-66, Test for Sound Absorption of Acoustical Materials in Reverberation Rooms American Society for Testing and Materials, Philadelphia.
8. ASTM E366-71, Measurement of Airborne Sound Insulation in Buildings, American Society for Testing and Materials, Philadelphia.
9. L. L. BERANEK, *Noise reduction*, McGraw-Hill Book Company, Inc., 1960, p. 298.